Intracerebral dynamics of sleep arousals: a combined scalp-intracranial EEG study

Yingqi Laetitia Wang, Tamir Avigdor, Sana Hannan, Chifaou Abdallah, François Dubeau, Laure Peter-Derex, Birgit Frauscher

Systems/Circuits

Intracerebral Dynamics of Sleep Arousals: A Combined Scalp–Intracranial EEG Study

Yingqi Laetitia Wang,[1]* Tamir Avigdor,[1]* Sana Hannan,[2] Chifaou Abdallah,[1] François Dubeau,[3] Laure Peter-Derex,[4] and Birgit Frauscher[1,5]

[1]Analytical Neurophysiology Lab, Montreal Neurological Institute, McGill University, Montreal, Quebec H3A 2B4, Canada, [2]Department of Biomedical and Life Sciences, Lancaster University, Lancaster LA1 4YW, United Kingdom, [3]Montreal Neurological Institute, McGill University, Montreal, Quebec H3A 2B4, Canada, [4]Centre de Médecine du Sommeil et des Maladies respiratoires, University Hospital of Lyon, Lyon 1 University, Lyon 69004, France, and [5]Analytical Neurophysiology Lab, Departments of Neurology & Biomedical Engineering, Duke University, Durham, North Carolina 27705

As an intrinsic component of sleep architecture, sleep arousals represent an intermediate state between sleep and wakefulness and are important for sleep–wake regulation. They are defined in an all-or-none manner, whereas they actually present a wide range of scalp-electroencephalography (EEG) activity patterns. It is poorly understood how these arousals differ in their mechanisms. Stereo-EEG (SEEG) provides the unique opportunity to record intracranial activities in superficial and deep structures in humans. Using combined polysomnography and SEEG, we quantitatively categorized arousals during nonrapid eye movement sleep into slow wave (SW) and non-SW arousals based on whether they co-occurred with a scalp-EEG SW event. We then investigated their intracranial correlates in up to 26 brain regions from 26 patients (12 females). Across both arousal types, intracranial theta, alpha, sigma, and beta activities increased in up to 25 regions ($p < 0.05$; $d = 0.06–0.63$), while gamma and high-frequency (HF) activities decreased in up to 18 regions across the five brain lobes ($p < 0.05$; $d = 0.06–0.44$). Intracranial delta power widely increased across five lobes during SW arousals ($p < 0.05$ in 22 regions; $d = 0.10–0.39$), while it widely decreased during non-SW arousals ($p < 0.05$ in 19 regions; $d = 0.10–0.30$). Despite these main patterns, unique activities were observed locally in some regions such as the hippocampus and middle cingulate cortex, indicating spatial heterogeneity of arousal responses. Our results suggest that non-SW arousals correspond to a higher level of brain activation than SW arousals. The decrease in HF activities could potentially explain the absence of awareness and recollection during arousals.

Key words: **high frequency; human; intracranial EEG; local; sleep; sleep arousals**

Significance Statement

Intrinsic to sleep architecture, sleep arousals are important for sleep–wake regulation. They are defined in an all-or-none manner, whereas they actually present various scalp-electroencephalography (EEG) patterns. Using simultaneous scalp and intracranial EEG in humans, we analyzed the intracranial activity during two arousal types marked on scalp-EEG, quantitatively categorized by whether they co-occurred with a scalp-EEG slow wave (SW). Non-SW arousals present prevalent higher frequency activity > 4 Hz, while SW arousals exhibit high-voltage SWs alongside fast activities. This work represents the first intracranial study of different nonrapid eye movement sleep arousals and provides a comprehensive description of local brain activities during both arousal types, serving as a foundation for future studies investigating regional behaviors during sleep–wake transition.

Received April 10, 2023; revised Feb. 5, 2024; accepted Feb. 12, 2024.

Author contributions: Y.L.W., T.A., S.H., L.P.-D., and B.F. designed research; Y.L.W., T.A., C.A., L.P.-D., and B.F. performed research; F.D., L.P.-D., and B.F. contributed unpublished reagents/analytic tools; Y.L.W., T.A., and B.F. analyzed data; Y.L.W. and B.F. wrote the paper.

This work was supported by the Natural Sciences and Engineering Research Council (NSERC) of Canada RGPIN-2020-04127 and RGPAS-2020-00021 to B.F., Salary award (Chercheur-boursier clinicien Senior) from the Fonds de Recherche du Québec – Santé (2021–2025) to B.F., Canada Graduate Scholarships-Master's from the NSERC to Y.L.W., and Fonds de recherché du Québec – Nature et technologies Funding for Master's students to Y.L.W.

*Y.L.W. and T.A. contributed equally to this work.

The authors declare no competing financial interests related to the study. Outside of the study, B.F. received honoraria for speaker's engagements/advisory board participation of UCB Pharma, Eisai, Paladin Labs, and UNEEG Medical, and has an ongoing active collaboration with Holberg EEG.

Correspondence should be addressed to Birgit Frauscher at birgit.frauscher@duke.edu.

https://doi.org/10.1523/JNEUROSCI.0617-23.2024

Introduction

Intrinsic to sleep architecture, sleep arousals are transient periods of increased vigilance level that occur around a hundred times every night without the sleeper's awareness or recollection (Schieber et al., 1971; Halász et al., 1979; Mathur and Douglas, 1995). They reflect an intermediate state between sleep and wakefulness and are defined as the shift of brain activity to higher frequencies in scalp-electroencephalography (EEG; Peter-Derex et al., 2015; Berry et al., 2020). Functionally, they may play a crucial role in sleep–wake regulation, allowing the brain to respond to important environmental cues while preserving sleep continuity (Boselli et al., 1998; Halasz et al., 2004; Bonnet and Arand, 2007; Latreille et al., 2020).

Sleep arousals have been defined as an all-or-none phenomenon (ASDA, 1992; Berry et al., 2020); however, arousals during nonrapid eye movement (NREM) sleep exhibit a wide range of activity patterns that differ in the amount of slow wave (SW) activity observed on the scalp-EEG (Schieber et al., 1971; Halász, 1998; Parrino et al., 2006). "Fast" arousals present prevalent higher frequency activity > 4 Hz, while "slow" arousals exhibit high-voltage SWs alongside fast activities. Despite the importance of arousals in sleep structure, the intracranial mechanisms leading to the scalp-EEG manifestation of different arousal types remain poorly understood.

Previous studies provided partial insights to this question: from "slow" to "fast" arousals, a weak to strong modification of muscle tone and cardiorespiratory rates was reported, suggesting that different arousal types represent a continuous spectrum of physiological activation and share a common brainstem involvement (Sforza et al., 1999, 2000; Terzano et al., 2002; Azarbarzin et al., 2014). Recent studies using stereo-EEG (SEEG) provided further insight. These recordings, performed exclusively in the presurgical evaluation of patients with focal drug-resistant epilepsy, offer the unique opportunity to record superficial and deep structures with high spatiotemporal resolution. They further enable evaluation of high-frequency (HF) activity which is difficult to distinguish on the scalp. When combined with polysomnography (PSG) and capitalizing on the channels without epileptic activity, SEEG can provide a thorough description of the intracranial activity underlying physiological sleep oscillations (Frauscher et al., 2020; von Ellenrieder et al., 2020). Using this method, a homogeneous activity was discovered in the thalamus during NREM arousals, suggesting a common subcortical correlate underlying all arousal types (Peter-Derex et al., 2015). In contrast, a highly heterogeneous activity was found across different cortical regions (Nobili et al., 2011; Peter-Derex et al., 2015; Ruby et al., 2021), indicating the activity variations during NREM arousals have a predominantly cortical origin. However, previous studies were limited as they lacked differentiation between arousal types and had small sample sizes ranging from four to eight patients (Nobili et al., 2011; Peter-Derex et al., 2015; Ruby et al., 2021). Investigating the regional activities during different arousal types is crucial to understanding the nature of sleep arousals. It could also offer valuable insights into the neural activity during pathological sleep–wake transitions such as NREM parasomnias.

In this study, we quantitatively categorized NREM sleep arousals into SW arousals and non-SW arousals based on whether they co-occurred with a scalp-EEG SW event and investigated their intracranial correlates in up to 26 brain regions from 26 patients. We explored (1) the regional activities during sleep arousals, (2) the intracranial differences between the two arousal types, and (3) the influence of sleep homeostatic pressure on their overnight occurrence. We hypothesized that (1) due to the heterogeneous cortical activity observed previously, NREM arousals show region-specific patterns (Nobili et al., 2011; Peter-Derex et al., 2015; Ruby et al., 2021); (2) non-SW arousals represent a higher level of cortical activation than SW arousals as assessed by their activity change, given the higher autonomic modifications reported previously (Sforza et al., 1999, 2000; Terzano et al., 2002; Azarbarzin et al., 2014); and (3) "slow" arousals are more likely to occur during the first half of the night when the sleep pressure is high (Terzano et al., 2002).

Materials and Methods

Patient selection

We reviewed medical charts of 55 consecutive patients (30 males, 25 females) with drug-resistant focal epilepsy, aged 16 years or older, who underwent combined intracerebral SEEG and PSG recordings as part of their presurgical epilepsy evaluation at the Montreal Neurological Institute and Hospital between Oct. 2013 and Oct. 2021. If a patient underwent more than one SEEG evaluation, the most recent evaluation was used. Exclusion criteria were (1) absence of SEEG channels with normal physiological activity, (2) absence of a well-identified seizure-onset zone (SOZ), (3) unreliable sleep and arousal scoring, (4) presence of an electroclinical seizure during the selected night of combined SEEG–PSG recordings, and (5) NREM arousal index (number of arousals per hour) exceeding the normative range (Mitterling et al., 2015). If asymptomatic electrographic seizures were present, a 30 min window, starting 15 min before the seizure onset and ending 15 min after the seizure offset, was excluded from the analysis. This study was approved by the Montreal Neurological Institute and Hospital Review Ethics Board (2014-183).

Intracranial and scalp-EEG recordings

Depth MNI (9 contacts, 0.5–1 mm in diameter, separated by 5 mm; 8 patients) or DIXI (10–15 contacts, 2 mm in diameter, separated by 1.5 mm; 18 patients) electrodes were implanted stereotactically using an image-guided system (ROSA Robotic or Medtronic Stealth). The scalp-EEG was recorded with subdermal thin wire electrodes at positions F4, C4, P4, F3, C3, P3, Fz, Cz, and Pz (except for one patient who had only F4, C4, F3, and C3; one patient who had only Fz, Cz, and Pz; and one patient who did not have F3). Electrooculography and chin electromyography electrodes were applied prior to the night of the sleep recording. Scalp-EEG channels were assessed using a bipolar montage, instead of the standard referential mastoid montage, as done in our previous studies. The reasons are as follows: (1) the mastoid electrode was not feasible for all patients due to the locations of implanted SEEG channels and the risk of contaminating the EEG activity with epileptic activity and SW anomalies and (2) bipolar montage was best suited for our study purpose to highlight local sleep activity (Frauscher et al., 2015a, 2020; Latreille et al., 2020; Peter-Derex et al., 2023b).

SEEG recordings were sampled at 2 kHz using the Harmonie EEG system (Stellate) for recordings prior to 2017 and the NeuroWorkbench EEG system (Nihon Kohden) for recordings obtained in 2017 and later. EEG signals were high-pass filtered at 0.1 Hz and low-pass filtered at 500 Hz in the Harmonie EEG system and high-pass filtered at 0.08 Hz and low-pass filtered at 600 Hz in the NeuroWorkbench EEG system. Intracranial channels were assessed in the bipolar montage with the neighboring contacts on the SEEG electrode.

Selection and localization of intracranial channels

Only SEEG channels with normal brain activity were included in the analysis; these were determined by a procedure described in our previous work (Frauscher et al., 2018a). Briefly, these channels are located outside the SOZ, inside a normal tissue as assessed by MRI, do not show interictal epileptic discharges throughout the SEEG investigation, and do not show a significant SW anomaly.

All patients underwent postimplantation imaging for anatomical localization of individual channels, which were determined using a

procedure described previously (Drouin et al., 2016; Frauscher et al., 2018a). SEEG channels were then grouped into 38 anatomical regions that were condensed from a brain segmentation template, which originally included 66 regions in the cortical gray matter (Landman and Warfield, 2012). Certain regions were merged to increase the number of channels in each region, which ultimately resulted in 38 anatomical regions (Frauscher et al., 2018b). We then combined the same regions from both hemispheres to increase the number of channels available per region, as there is no evidence suggesting that there are differences in EEG power spectra between hemispheres (Frauscher et al., 2018a). Finally, we excluded any region that contained less than three channels or were available in less than three patients.

Sleep and arousal scoring

Sleep scoring was performed manually in 30 s epochs using the scalp-EEG, blind to SEEG data, by a board-certified neurophysiologist (B.F.), according to the American Academy of Sleep Medicine (AASM) criteria (Berry et al., 2020). Arousals are defined as an abrupt shift of EEG frequency including alpha, theta, and/or frequencies >16 Hz (but not spindles) lasting at least 3 s, with at least 10 s of stable sleep preceding the change (Berry et al., 2020). The end of arousals was determined as either the clear reappearance of a sleep pattern, including the disappearance of rapid activities and the reappearance of a slower background rhythm, and sleep features (vertex waves, spindles) or, for arousals preceding an epoch of wakefulness, by the onset of this epoch.

Unambiguous sleep arousals were manually scored by a board-certified neurophysiologist (L.P.-D.) on Fz–Cz and in five patients on F3–C3, Cz–Pz, or Fz–P4 due to artifacts in Fz–Cz, including those preceding awakenings or stage shifts. We then randomly selected 10% of the arousals of each patient and created the same number of nonarousal events, which were segments placed randomly during the nonarousal part of the recordings and which had an identical duration as the selected arousals. After that, the arousals and nonarousals were independently scored by two board-certified neurophysiologists (B.F. and C.A.) without knowledge of the markings by L.P.-D. The kappa values were 76.8% between L.P.-D. and B.F. and 89.2% between L.P.-D. and C.A. These rates were considered excellent in the clinical context (Kaufman and Rosenthal, 2009).

Temporal windows of interest

We assessed the scalp-EEG and intracranial activities during three temporal windows, the arousal onset, arousal body, and arousal offset (Fig. 2). The temporal windows were defined using the scalp-EEG marking of arousals, and the intracranial activities were computed using these time windows (TWs). The arousal onset was defined as the first 3 s window of the arousal, because (1) this was used in previous studies on sleep arousals (Peter-Derex et al., 2015, Ruby et al., 2021) and (2) the American Sleep Disorders Association defined the minimum duration of arousals to be 3 s (ASDA, 1992). The arousal body was defined as the period immediately after the onset until the end of the arousal. The division into the arousal onset and body was based on the observation of a strong delta increase at the beginning of some arousals compared with the arousal body (Peter-Derex et al., 2015, 2020). To explore the intracranial activities during the return to sleep immediately after the arousal, we defined the 3 s window after the end of the arousal as the arousal offset. Since sleep arousals are defined as a transient change in the current brain state, the baseline segment for the arousal onset, body, and offset was selected individually for each arousal from every channel, instead of having the same baseline for all arousals. They were defined as the 10 s period of continuous sleep from −12 to −2 s where 0 s is the arousal start time. The duration of 10 s was decided based on the AASM criteria that state that at least 10 s of stable sleep must precede the arousal (Berry et al., 2020). We chose to end the baseline at −2 s with respect to the arousal onset because previous studies reported that the delta activity increased in certain cortical areas during the 1–2 s before the onset of arousals on the scalp-EEG (Nobili et al., 2011; Peter-Derex et al., 2015). Excluding the 2 s prior to arousals thus avoided the potential contamination of the baseline segment by the early intracranial activity associated with arousals.

Arousal selection

For this study, 1,646 sleep arousals from NREM stages N2 and N3 were included and analyzed together as NREM arousals. Because we wanted to study the delta activity (0.5–4 Hz) that included frequencies at 0.5 Hz during the arousal body, we only included arousals with a duration of 5 s or longer to ensure that the arousal body lasted for at least 2 s. We thus excluded arousals that were shorter than 5 s ($n = 18\%$ of all included arousals). We further excluded arousals whose baselines occurred in a different sleep stage to the arousal itself ($n = 6\%$), crossed two sleep stages ($n = 3.4\%$), or overlapped with another arousal ($n = 1.6\%$), so that the activity change during the arousals was not affected by the inherent changes in the brain activity which occur during the transition between different sleep stages.

Classification of arousals

We classified arousals into SW and non-SW arousals. If the arousal intersected temporally with a SW event detected on any of the scalp channels specified below, it was classified as a SW arousal. If there was no co-occurring SW event, the arousal was defined as a non-SW arousal.

SW detector. SW events were automatically detected on scalp channels Fz–Cz, F3–C3, C3–P3, F4–C4, C4–P4, and Cz–Pz during N2 and N3 sleep. Using a bipolar montage reduces the overall EEG amplitude compared with the referential montage. This reduction significantly impacts the SW activity, with the potential for an up to 75% decrease in the Fz–Cz channel compared with the C4–M1 channel (Kemp et al., 2013). As a result, we adjusted the amplitude detection criteria for SW events as done in our previous work (Latreille et al., 2023). In brief, the data were first filtered within the 0.3–4 Hz range, and all successive positive-to-negative zero crossings were identified. We then included SW with a duration of 0.125–3 s. After that, we lowered the amplitude thresholds by 50–60% to account for the potential decrease of the EEG amplitude in the bipolar montage. Visual confirmation was then performed independently by neurophysiologists, blinded to the patients' diagnosis, on a subset of patients with randomly selected arousals. Based on the visual assessment, the peak-to-peak amplitude was set at 40 μV, and the negative peak amplitude was set at 20 μV to ensure the best detection of SW events (Latreille et al., 2023).

Quantification of activity changes during arousals

Both the scalp-EEG and SEEG signals were bandpass filtered at 0.3–300 Hz. The scalp-EEG signal was additionally preprocessed with a 60 Hz notch filter. To quantify the activity change during each temporal window, we computed the ratio of the mean band power during the TW of interest versus that during the baseline, in the delta (0.5–4 Hz), theta (4–8 Hz), alpha (8–13 Hz), sigma (10–16 Hz), beta (17–30 Hz), gamma (30–80 Hz), and HF (80–250 Hz) ranges. The power spectral density (PSD) was estimated using the Welch method (Hamming window, 2 s window length, 50% overlap). Note that the PSD of gamma and HF activities was only computed on the SEEG signal but not on the scalp-EEG, as these activities were challenging to distinguish from the muscle artifacts on the scalp which would lead to unreliable quantification. All signal processing and power spectrum analyses were performed using the software Brainstorm (Tadel et al., 2011).

We further explored the sleep-related and wake-related properties of every region in each TW of interest (onset, body, and offset) by computing the wake-related ratio defined as the average of theta, alpha, and beta activity ratio (the ratio means: power during the TW of interest/power during baseline) versus the delta activity ratio during the TW of interest. This measure is based on previous findings that the delta activity is associated with sleep and theta, alpha, and beta activities are associated with wakefulness (Berger, 1929; Jasper and Penfield, 1949; De Gennaro et al., 2001; Cote et al., 2002; Buzsáki, 2011; Adamantidis et al., 2019). It allows us to explore whether the brain region becomes more sleep-related or wake-related during sleep arousals relative to the prearousal baseline.

Statistical analysis

Overnight distribution and duration of arousals. We computed the arousal indices of SW and non-SW arousals during the first and second half of the night in each patient. We then conducted a repeated-measures

ANOVA with two within factors: arousal type (SW, non-SW arousals) and part of sleep (first half, second half).

We compared the duration of the two types of arousals using the Mann–Whitney *U* test for nonparametric data. The effect size Cliff's *d* was computed.

Activity changes during arousals. To analyze the intracranial activity changes during each arousal type, we pooled from all patients the power ratio (power during TW of interest/power during baseline) of individual frequency bands, as well as the wake-related ratio, from all channels in each anatomical region. Similarly, to analyze the scalp-EEG activity changes during each arousal type, we pooled from all patients the power ratio from the channels on which the arousals were marked.

After that, the pooled ratios were natural log transformed to approximate a normal distribution. Since each patient had different numbers of every arousal type and different numbers of channels in each region, the distribution was weighted according to the number of data points that each patient contributed to the dataset, in order to ensure that the distribution mean was not biased by a specific patient (Peter-Derex et al., 2023a). A one-sample *t* test against zero was then performed to assess (1) whether there was a significant intracranial activity change in each region during arousals ($\alpha < 0.05$), (2) whether there was a significant scalp activity change ($\alpha < 0.05$), and (3) in terms of wake-related ratio, whether the change in the fast activity (theta, alpha, and beta) is significantly higher than the change in the delta activity, or the opposite.

All *p* values were corrected with the false discovery rate procedure. For intracranial analysis of the individual bands, 7 frequency bands × 3 TW × (26 regions for SW arousals and 25 regions for non-SW arousals) = 7 × 3 × 26 + 7 × 3 × 25 = 1,071 *p* values were corrected in total. The *p* values of the wake-related ratio were corrected separately: 3 × 26 + 3 × 25 = 153 *p* values were corrected. For the scalp-EEG analysis, 7 × 3 + 7 × 3 = 42 *p* values were corrected for individual bands, and 1 × 3 + 1 × 3 = 6 *p* values were corrected separately for the wake-related ratio.

If the activity change after correction was statistically significant, the effect size Cohen's *d* of the one-sample *t* test of each region was computed. A positive effect size of individual frequency bands means an activity increase in the region and vice versa. Regarding wake-related ratio, a positive value means a stronger activity change in the theta to beta activity range compared with that in the delta range and vice versa. Small, medium, and large effect sizes were suggested as Cohen's $d = 0.2$, 0.5, and 0.8, respectively.

Activity comparisons between arousal types. To directly compare the activities between two arousal types, we conducted a Welch's *t* test between SW and non-SW arousals using the data of all channels in each brain region during each TW ($\alpha < 0.05$). *p* values were corrected with the false discovery rate procedure (25 regions × 2 arousal types × 3 TW = 150 pairs of *p* values corrected for each frequency band). Effect sizes were then computed in Cohen's *d* for significant comparisons.

Results

Patient and arousal information

Twenty-six patients (12 females) with a mean age of 35.5 ± 11.2 years met our selection criteria and were therefore included (Fig. 1). Patient demographic and clinical characteristics are provided in Table 1. We included 613 SW arousals and 563 non-SW arousals (Fig. 2). After the anatomical localization of the SEEG channels, we identified a total of 26 regions to study SW arousals and 25 regions to study non-SW arousals (Fig. 3).

The median duration of SW arousals was 8.2 s (range, 5.0–25.3 s) and 7.5 s (range, 5.0–25.4 s) for non-SW arousals. The duration of non-SW arousals was significantly shorter than that of SW arousals (Mann–Whitney *U* test, $U = 374{,}520$; $p = 0.02$; Cliff's $d = 0.54$).

The two-way repeated-measures ANOVA to assess the overnight distribution of arousals revealed no significant main effects or interactions, indicating that SW and non-SW arousals did not distribute differently across the night (main effect of arousal type: $F_{(1,25)} = 0.145$, $p = 0.707$; main effect of half of sleep: $F_{(1,25)} = 3.467$, $p = 0.074$; interaction between two factors: $F_{(1,25)} = 0.272$, $p = 0.607$).

Delta activity shows a widespread increase during SW arousals and a widespread decrease during non-SW arousals

The intracranial delta activity during the two arousal types aligns with the scalp-EEG delta activity even in the medial and deep brain regions. During SW arousals, we reported an early widespread increase in delta band power across all the five brain lobes that became more locally confined to temporoparietal regions during the body (onset and body: $p < 0.05$ in 22 and 5 regions; $d = 0.10$–0.39 and $d = 0.05$–0.15; Fig. 4; Tables 2, 3). On the scalp, we observed a similar increase during the onset and no change during the body (onset, $p < 0.05$; $d = 0.31$; body, $p > 0.05$).

During non-SW arousals, we observed an increase in the delta activity across the five brain lobes during the onset, followed by a widespread decrease across the five lobes during the body (onset increase: $p < 0.05$ in 11 regions, $d = 0.10$–0.29; body decrease: $p < 0.05$ in 19 regions, $d = 0.10$–0.30; Fig. 4; Tables 2, 3). On the scalp, the delta activity similarly showed an increase during the onset and a decrease during the body ($p < 0.05$; $d = 0.15$ and 0.11).

During the arousal offset, the delta power decreased after both arousal types across all the five brain lobes (SW arousals: $p < 0.05$ in 18 regions, $d = 0.10$–0.69; non-SW arousals: $p < 0.05$ in 21 regions, $d = 0.12$–0.32; Fig. 4; Tables 2, 3). These patterns showed on the scalp as no change during the SW arousal offset ($p > 0.05$) and a decrease during the non-SW arousal offset ($p < 0.05$; $d = 0.27$).

By directly comparing the activities between SW and non-SW arousals, we observed that the delta activity in many regions across the five lobes differed significantly between the two arousal types ($p < 0.05$ for all; $d = 0.12$–0.50; Table 4).

Theta, alpha, sigma, and beta activities show widespread increases during both arousal types

During both arousal types, theta, alpha, sigma, and beta power increased in many regions across all the five brain lobes during the onset. As the arousals progressed into the body phase, theta, alpha, and sigma activities continued to increase, albeit in fewer regions, while the beta activity expanded to increase in more regions. After that, during the offset, theta, alpha, and sigma activities decreased widely across the five lobes, while the beta activity returned to baseline in the majority of regions (Fig. 5; Tables 2, 3).

In detail, for SW arousals, theta, alpha, sigma, and beta power increased in 19, 25, 22, and 10 regions during the onset ($p < 0.05$ for all; $d = 0.06$–0.60; $d = 0.04$–0.30; $d = 0.06$–0.34; and $d = 0.06$–0.25). After that, theta, alpha, and sigma increased in 11, 16, and 19 regions during the body, while beta increased in 19 regions ($p < 0.05$ for all; $d = 0.06$–0.28; $d = 0.07$–0.23; $d = 0.08$–0.25; and $d = 0.06$–0.33). During the offset, theta, alpha, and sigma power widely decreased in 17, 15, and 15 regions ($p < 0.05$ for all; $d = 0.07$–0.43; $d = 0.06$–0.23; $d = 0.08$–0.25), while the beta activity returned to baseline in most of the regions.

Similarly, theta, alpha, sigma, and beta activities increased in 9, 16, 14, and 12 regions across the five lobes during the non-SW arousal onset ($p < 0.05$ for all; $d = 0.11$–0.27; $d = 0.09$–0.63; $d = 0.08$–0.47; and $d = 0.08$–0.40). After that, theta, alpha, and sigma power increased in 4, 10, and 9 regions ($p < 0.05$ for all; $d = 0.10$–0.20; $d = 0.10$–0.49; $d = 0.11$–0.37), while beta increased in 16 regions during the body ($p < 0.05$ for all; $d = 0.11$–0.45). Then, theta, alpha, and sigma activities showed a widespread

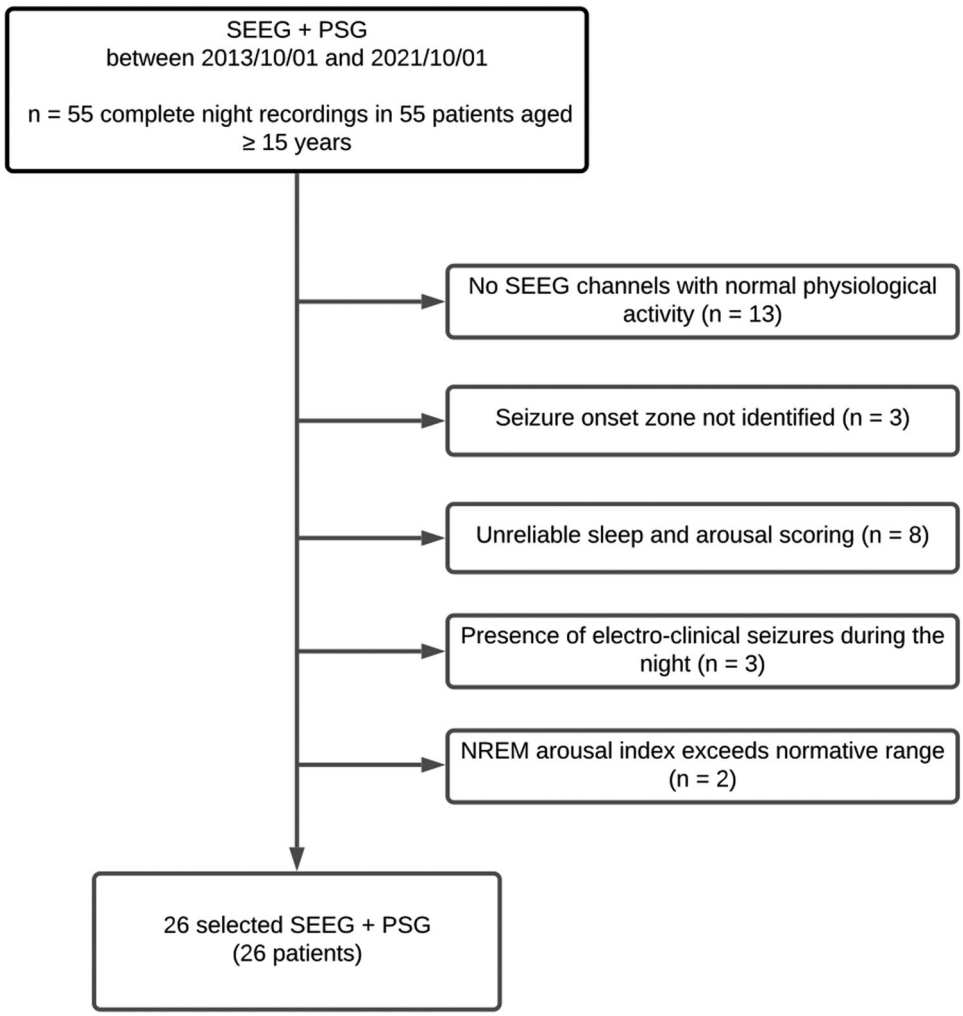

Figure 1. Flowchart of patient selection.

decrease across the five lobes in 19, 17, and 20 regions ($p < 0.05$ for all; $d = 0.09$–0.35; and $d = 0.12$–0.49), while the beta activity returned to baseline in all regions except two.

The comparison of the activities between the two arousal types revealed that the increase in theta, alpha, sigma, and beta activities was lower during SW arousals than that during NW arousals in multiple temporo-parieto-occipital regions ($p < 0.05$ for all; $d = 0.14$–0.42). In addition, the decrease in theta, alpha, and sigma activities was weaker in many regions across the five brain lobes during the offset of SW arousals ($p < 0.05$ for all; $d = 0.13$–0.68), while the beta activity during offset did not differ between the two arousal types (Table 4).

Note that these increases were not explained by the number of channels in the respective brain regions. The general intracranial activity pattern also manifested on the scalp-EEG.

Gamma and HF activities decrease in many regions during both arousal types

Across both arousal types, gamma and HF activities decreased in many regions across the five brain lobes during the onset. They then continued to decrease during the body, only in fewer regions. During the offset, they continued to decrease or returned to baseline (Fig. 6; Tables 2, 3).

In detail, during SW arousals, gamma and HF activities decreased in 17 and 18 regions during the onset ($p < 0.05$ for all; $d = 0.07$–0.44; and $d = 0.10$–0.43). They then decreased primarily in the fronto-parieto-occipital regions during the body ($p < 0.05$ in 7 and 10 regions; $d = 0.06$–0.28; and $d = 0.09$–0.24).

Regarding non-SW arousals, we observed an early decrease in gamma and HF activities both in 11 regions across the five lobes during the onset ($p < 0.05$ for all, $d = 0.13$–0.39 and $d = 0.14$–0.34). After that, four and seven regions showed a decrease in gamma and HF activities during the body ($p < 0.05$ for all; $d = 0.10$–0.24; and $d = 0.12$–0.27). During the offset, gamma power returned to baseline except in the parietal operculum ($p < 0.05$; $d = 0.18$), while HF activities continued to decrease in the five temporoparietal regions ($p < 0.05$; $d = 0.11$–0.27).

Comparing the activities between SW and non-SW arousals showed that gamma and HF activities only differed in less than five regions across the five lobes between the two arousal types ($p < 0.05$ for all; $d = 0.15$–0.44) (Table 4). The gamma decrease in the inferior occipital gyrus and occipital pole was weaker during SW arousals ($p < 0.05$; $d = 0.27$), and the HF decrease in the cuneus was stronger during the onset of SW arousals ($p < 0.05$; $d = 0.44$).

SW arousals show sleep-related properties during the onset, while non-SW arousals show persistent wake-related properties

We further explored whether different brain regions became more sleep related or wake related compared with the prearousal baseline (Fig. 7; Tables 2, 3). SW arousals showed a widespread

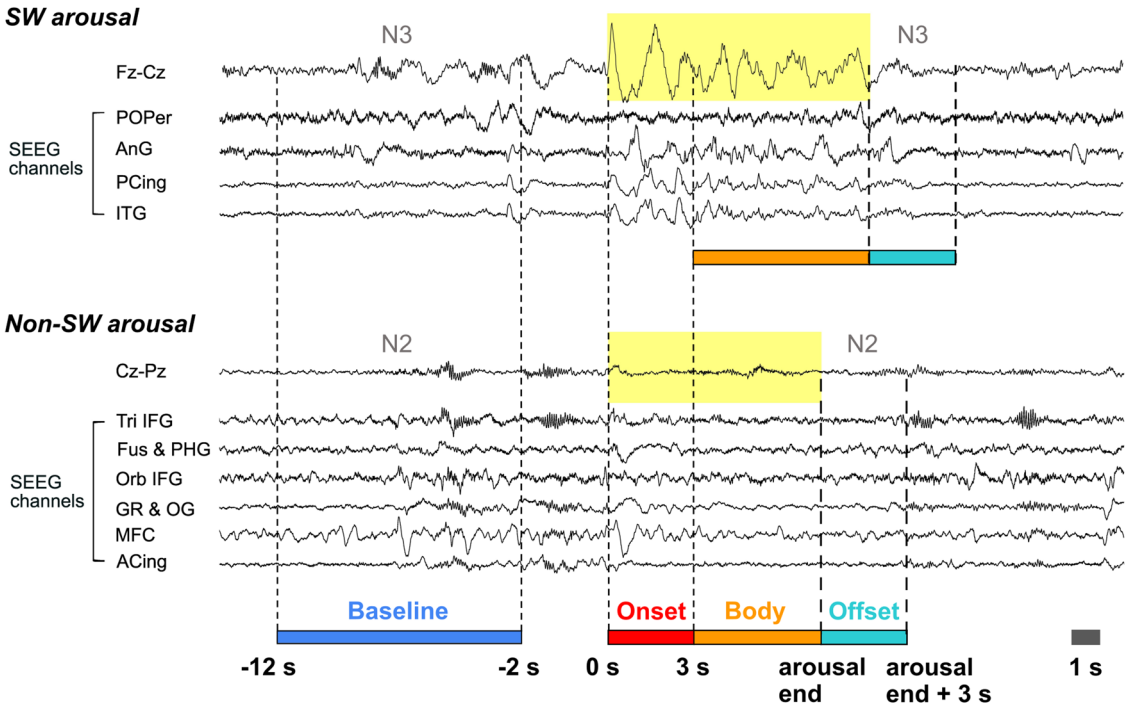

Figure 2. Schematic of temporal windows of interest and arousal types. Representative examples of SW and non-SW arousals taken from patients 9 and 24 are shown, recorded on the scalp-EEG and SEEG. Arousals were marked on the scalp-EEG using Fz–Cz for patient 9 and Cz–Pz for patient 24. The remaining channels are SEEG channels. The onset, body, and baseline segments are indicated by the dashed lines and arrows. The yellow marking represents the arousal segment. The NREM sleep stage before and after the arousal was indicated above each example. Here, the SW arousal exhibits delta activity throughout its onset and body with superimposed fast activity, while the non-SW arousal shows fast activity throughout. POper, parietal operculum; AnG, angular gyrus; PCing, posterior cingulate; ITG, inferior temporal gyrus; ACing, anterior cingulate gyrus; Tri IFG, triangular part of the inferior frontal gyrus; Fus & PHG, fusiform and parahippocampal gyrus; Orb IFG, orbital part of the inferior frontal gyrus; GR & OG, gyrus rectus and orbital gyrus; MFC, medial frontal cortex.

sleep-related activity pattern during the onset, which then turned to a widespread wake-related pattern during the body (onset and body: $p < 0.05$ in 17 and 21 regions; $d = 0.05$–0.36; and $d = 0.05$–0.50). During the offset, 15 regions were wake-related ($p < 0.05$; $d = 0.09$–0.35).

Non-SW arousals showed a wake-related activity pattern throughout their duration. Across all five lobes, 12 regions across the five lobes were wake-related during the onset, and 24 regions were wake-related during the body ($p < 0.05$ for all, onset: $d = 0.11$–0.34; body: 0.15–0.55).

A similar pattern as described for the SEEG manifested on the scalp-EEG. Regarding SW arousals, we observed a sleep-related activity pattern during the onset and a wake-related pattern during the body and offset ($p < 0.05$ for all; $d = 0.12$, 0.27, 0.12). For non-SW arousals and their offset, a wake-related pattern was observed during the body and offset ($p < 0.05$; $d = 0.27$ and 0.23).

The wake-related property was weaker during SW arousals than that during non-SW arousals in up to 15 regions across the five lobes ($p < 0.05$; $d = 0.10$–0.72).

Intracranial activity during sleep arousals exhibit spatial heterogeneity

While the intracranial activity of each frequency band exhibited a general pattern across brain regions which was also observed on the scalp-EEG, multiple regions exhibited unique activities (Figs. 4–7). Throughout SW arousals, the parietal operculum, hippocampus, planum temporale, and middle cingulate cortex showed no increases in the delta activity; in fact, the parietal operculum, planum temporale, and middle cingulate even showed a decrease during the body ($p < 0.05$ for all; $d = 0.18$; $d = 0.28$; and $d = 0.40$). The middle cingulate also showed no increase in the theta, alpha, sigma, or beta bands ($p > 0.05$). In addition, the fusiform and parahippocampal gyri, hippocampus, amygdala, middle temporal gyrus, superior temporal gyrus, and posterior insula showed no decreases in neither gamma nor HF band power, but only an increase in HF power in the middle temporal gyrus ($p < 0.05$; $d_{onset} = 0.26$; $d_{body} = 0.31$), superior temporal gyrus ($p < 0.05$; $d_{body} = 0.20$), and posterior insula ($p < 0.05$; $d_{onset} = 0.12$; $d_{body} = 0.24$). Interestingly, the parietal operculum and planum temporale showed a unique wake-related activity pattern during the onset ($p < 0.05$; $d = 0.13$ and 0.35), coexisting with other sleep-related regions.

For non-SW arousals, the hippocampus, amygdala, and posterior insula showed no increases in theta, alpha, sigma, or beta power; instead, the theta activity decreased in the hippocampus and amydala ($p < 0.05$ for all, hippocampus: $d_{onset} = 0.43$, $d_{body} = 0.34$; amygdala: $d_{body} = 0.53$). In gamma and HF bands, the supplementary motor cortex, hippocampus, amygalda, superior temporal gyrus, middle temporal gyrus, inferior temporal gyrus, posterior cingulate, and posterior insula showed no change throughout non-SW arousals ($p > 0.05$).

Discussion

Although sleep arousals have been defined as an all-or-none phenomenon, they actually present a wide range of scalp-EEG activity patterns. With the unique setup of combined SEEG–PSG, we categorized NREM arousals into SW arousals and non-SW arousals and studied their intracranial activities. Our main findings were as follows: (1) across both arousal types, theta to beta activities showed a widespread increase across many brain regions, while gamma and HF activities decreased in many regions; (2) delta activity increased widely during SW arousals,

Table 1. Patient demographics and clinical information

ID	Age (yr)	Sex	Epilepsy diagnosis	Seizure-onset zone	MRI	Antiepileptic drugs (mg/d)	Anatomical regions of channels with physiological activity	No. of arousals (SW; non-SW)
1	41	F	R + L mesial temporal	R + L HPC + Amg and L fusiform gyrus and heterotopia	Periventricular nodular heterotopia	CLO (25), LEV (3,000)	Orb IFG, ACing, GR & OG, FOper, PCing, AnG, SPL, Fus & PHC, ITG, MTG, STG	4; 13
2	37	M	Bilateral temporal	L temporal neocortex + R mesial temporal	Periventricular nodular heterotopia	CBZ (1,400), LEV (3,000), CLO (10)	GR & OG, FOper, Orb IFG, ACing, Tri IFG	18; 20
3	47	M	L temporo-insular	L anterior temporal lobe + AIns	Normal	CBZ (1,200)	GR & OG, ACing, FOper, Tri IFG, PCing, AnG, Fus & PHG, ITG	26; 15
4	37	M	L temporo-insular	L temporal mesial and neocortical + PIns	Normal	CLO (30), CBZ (600), TPM (200)	GR & OG, Orb IFG, Cu, AnG	8; 34
5	57	F	R insular	R insula	Surgical bed (temporal)	LAM (200) CLO (20)	MFC, FOper, Orb IFG, MFG, AnG, COper, POper	12; 33
6	53	M	R mesial temporal	R temporo-occipital + R temporal mesial	Normal	OXC (1,800), LEV (1,000)	PCu, PCing, SMG, Cu, CC	7; 6
7	34	F	L temporo-occipital	L basal temporo-occipital cortex	Normal	CBZ (1,200), CLO (20), LAM (200)	Amg, TP & PP, POper, AnG, PCing, ITG	84; 13
8	36	M	Bilateral neocortical temporal	L + R temporal neocortex	L HPC atrophy	OXC (1,800), LEV (3,000), LAM (400)	IOG & OP, LG & OFG	6; 29
9	38	M	L temporo-occipital	L posterior HPC, LG, and Cu	L posterior temporal atrophy and gliosis	LEV (3,000), PHT (350), Clo (40)	GR & OG, FOper, Tri IFG, PCu, SMG, MCing, Oper IFG, MFG	2; 41
10	39	M	Bilateral temporal	L + R temporal mesial and neocortical	R HPC atrophy	VPA (2,000), CLO (30), LEV (3,000)	ACing, AIns, MCing, SMC	1; 46
11	27	F	L occipital	L lateral temporo-occipital cortex	L lateral occipital FCD	LAM (300), CBZ (400)	HPC, TTG, PCing, AnG, PCu, MSG, Cu	25; 21
12	22	M	Bilateral mesial temporal	L and R HPC + Amg	Bilateral mesial temporal sclerosis	CBZ (1,000), LAM (400), LEV (2,500)	GR & OG, FOper, Fus & PHG, IOG & OP	0; 28
13	29	M	L mesial temporal	L HPC + Amg	L left mesial temporal sclerosis + L frontal FCD	CBZ (1,200), CLO (20)	MFC, ACing, MFG	4; 20
14	24	M	Bilateral temporal mesial	L and R HPC + Amg	R HPC atrophy and L HPC malformation	CLO (15)	GR & OG, FOper, PCing, AnG, GR & OG, POper, TTG, SMG	7; 9
15	30	F	Bilateral temporal mesial	L and R HPC + Amg (R > L)	Normal	OXC (1,800), PHE (125), CLO (20), TPM (25)	MTG, ACing, MCing, SMC, PCing, POper, PCu, AnG	17; 5
16	26	F	L neocortical temporal	L temporal posterior neocortex + junction of temporal and inferior parietal areas	L hemispheric polymicrogyria + surgical bed (L orbitofrontal + temporal)	LAM (200), LEV (2,500), CBZ (800)	ACing, mSFG	25; 1
17	47	M	R temporoparietal	R posterior temporal and parietal neocortex	R postsurgical defect (anterior temporal resection) + R ischemic frontal lesion	LEV (4,000), LAM (200), CLO (20), ZNZ (200)	MCing, HPC, Fus & PHG	8; 31
18	61	F	L temporomesial and basal	L Amg, HPC, and fusiform gyrus	Ischemic lesion next to L lateral ventricle + HPC atrophia	BRV (100), LAC (150), PER (8), VEN (112.5)	GR& OG, FOper, Orb IFG, Tri IFG, ACing, AIns, MFG	11; 60
19	21	F	R mesial temporal	R HPC 1 Amg	Normal	CLO (5), LAM (500), AM (75)	Amg, TP & PP, PCing, ITG, MTG, ACing, Tri IFG, AIns, Orb IFG, PIns, TTG, POper, SMG	31; 2
20	32	M	L fronto-temporo-insular	L insula + temporal ± frontal	L temporal encephalomalacia	LEV (1,500), LAC (200), CLO (30)	mPG, PCing, MCing, Cu, PCu	2; 81
21	26	F	L mesial and basal temporal	R HPC 1 Amg 1 fusiform gyrus	Normal	LAC (200), PER (8), LAC (250), LAM (275)	PIns, PT, TTG, STG, HPC, Fus & PHC, MTG, AnG	59; 25
22	25	M	R frontal	R posterior orbitofrontal cortex and AIns	Normal	LAC (150), CLO (10), citalopram (10)	Tri IFG, ACing, Fus & PHC, MTG, MFC, FOper, GR & OG, Orb IFG	64; 1
23	18	F	R occipitotemporal	R occipitotemporal cortex	Normal	None (all AEDs held)	ITG, Cu, AnG, Su & M OG	13; 8
24	32	M	Bilateral mesial temporal	L hippocampal formation	L para-HPC lesion	None (all AEDs held)	GR & OG, FOper, Tri IFG, PIns, PCu, AnG, Fus & PHG, TTG, STG, IOG & OP, Su & M OG, MTG, ITG	102; 8
25	43	F	R insular	R AIns	Severe bilateral frontal atrophy	CLO (30), OXC (2,100), LOR (5)	MFC, ACing, SMC, GR & OG, FOper, Orb IFG, AIns, MFG, mSFG, Amg, PIns, TTG, PT, STG, PG, PIns, POper, SMG, Cu, IOG & OP, AnG, Fus & PHG, ITG, MTG, PCu	30; 13
26	42	M	L temporal	Widespread neocortical with maximum involvement of posterior temporo-occipital cortex	Hypersignal in left side of lower pons + possible lesion in fusiform gyrus	CBZ (1,200), LEV (1,000), LOR (4)	HPC, ITG, IOG & OP, TTG, PT, GR & OG, FOper, Orb IFG, AIns, MFG, PCing, AnG	47; 0

Medication abbreviations: AM, amitriptyline; BRV, brivaracetam; CBZ, carbamazepine; CLO, clonazepam; LAC, lacosamide; LAM, lamotrigine; LEV, levetiracetam; LOR, lorazepam; OXC, oxcarbazepine; PER, perampanel; PHE, phenytoine; TPM, topiramate; VEN, venlafaxine; VPA, sodium valproate; ZNS, zonisamide. Anatomical abbreviations: ACing, anterior cingulate; AIns, anterior insula; Amg, amygdala; AnG, angular gyrus; CC, calcarine cortex; COper, central operculum; Cu, cuneus; FOper, frontal operculum; Fus & PHG, fusiform and parahippocampal gyrus; GR & OG, gyrus rectus and orbital gyrus; HPC, hippocampus; IOG & OP, inferior occipital gyrus and occipital pole; ITG, inferior temporal gyrus; L, left; LG & OFG, lingual gyrus and occipital fusiform gyrus; MCing, middle cingulate; MFC, medial frontal cortex; MFG, middle frontal gyrus; mPG, medial segment of precentral gyrus; mSFG, medial segment of superior frontal gyrus; MTG, middle temporal gyrus; Orb IFG, orbital part of inferior frontal gyrus; Oper IFG, opercular part of inferior frontal gyrus; PCing, posterior cingulate; PCu, precuneus; PG, precentral gyrus; PIns, posterior insula; POper, parietal operculum; PT, planum temporale; R, right; SMC, supplementary motor cortex; SMG, supramarginal gyrus; SPL, superior parietal lobule; STG, superior temporal gyrus; Su & M OG, superior and middle occipital gyri; TP & PP, temporal pole and planum polare; TTG, transverse temporal gyrus; Tri IFG, triangular part of inferior frontal gyrus.

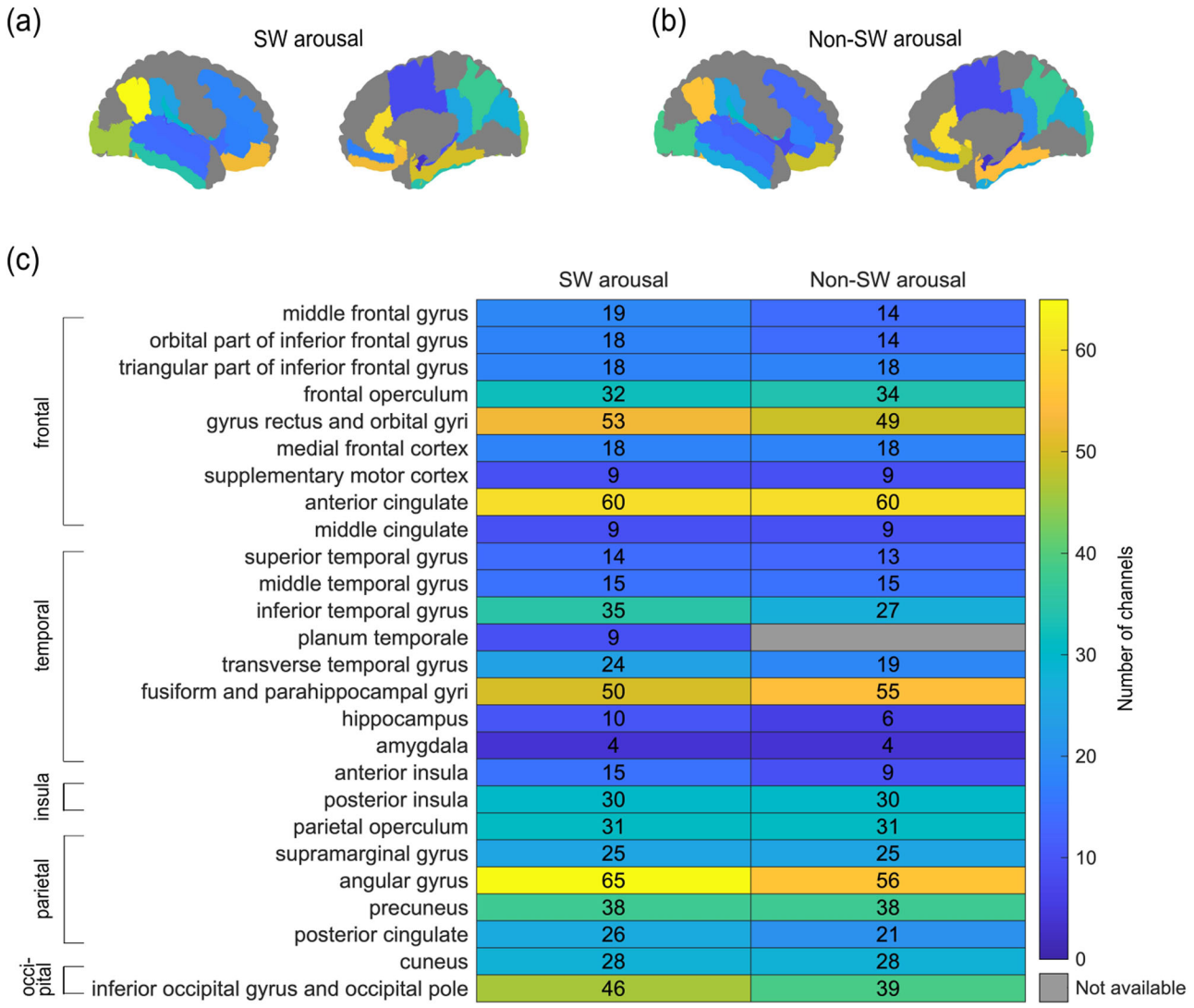

Figure 3. Localization of channels with physiological activity. ***a***, Number of channels with physiological activity that were selected in each anatomical region for SW arousals. ***b***, Number of channels with physiological activity in each region for non-SW arousals. ***c***, Number of channels included in each region for the two arousal types. Regions are listed in the following order: frontal lateral, frontal mesial, temporal lateral, temporal mesial, insula, parietal lateral, parietal mesial, occipital mesial, and occipital lateral areas. The channels for each region were grouped together from both hemispheres. There were 26 and 25 regions used to study SW and non-SW arousals.

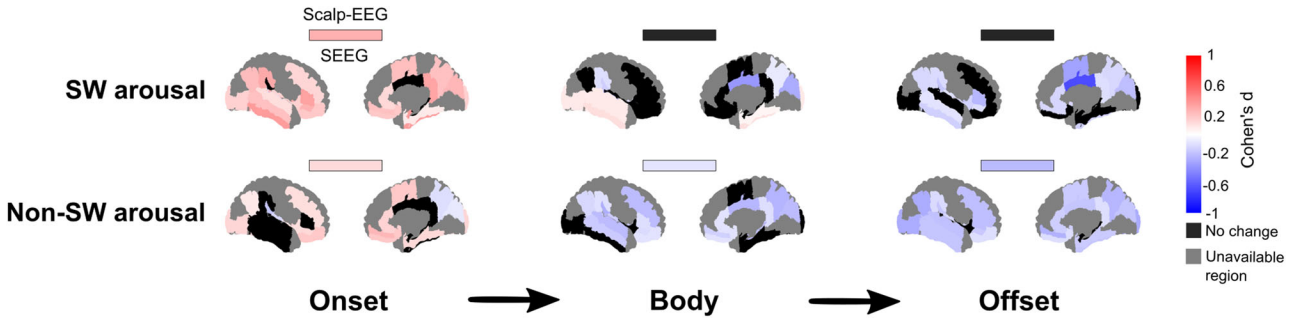

Figure 4. Delta activity widely increases during SW arousals and widely decreases during non-SW arousals. The color represents the effect size of the change in delta band power relative to baseline on the scalp-EEG (bar) and SEEG (brain visualizations) during the arousal onset, body, and offset of SW and non-SW arousals. Red represents an increase in delta power, while blue represents a decrease in delta power. Regions that were available in <3 patients are marked in gray, and regions with no significant change in delta power are in black. We observed that many regions showed a delta increase during SW arousals and the onset of non-SW arousals, yet many regions showed a delta decrease during the body of non-SW arousals.

whereas it decreased widely during non-SW arousals; (3) a sleep-related activity pattern dominated the onset of SW arousals, while a wake-related pattern persisted throughout non-SW arousals; and (4) despite a common arousal signature, a unique activity was observed locally in some regions, indicating spatial heterogeneity of arousal responses.

Table 2. *p* values of scalp-EEG and SEEG activities during SW arousals relative to baseline

		Delta (0.5–4 Hz)			Theta (4–8 Hz)			Alpha (8–13 Hz)			Sigma (10–16 Hz)			Beta (17–30 Hz)			Gamma (30–80 Hz)			High frequency (80–250 Hz)			Wake-related ratio		
		Onset	Body	Offset	Onset	Body	Offset	Onset	Body	Offset	Onset	Body	Offset	Onset	Body	Offset	Onset	Body	Offset	Onset	Body	Offset	Onset	Body	Offset
Scalp	Scalp-EEG	<0.001***	0.436	0.071	<0.001***	0.004**	<0.001***	<0.001***	<0.001***	<0.001***	<0.001***	0.281	<0.001***	<0.001***	<0.001***	<0.001***	N/A	N/A	N/A	N/A	N/A	N/A	0.004**	<0.001***	0.004**
Frontal	Middle frontal gyrus	<0.001***	0.309	0.388	<0.001***	0.445	0.297	<0.001***	0.361	0.919	<0.001***	0.029*	0.766	<0.001***	<0.001***	0.037*	<0.001***	0.109	0.568	<0.001***	0.005**	0.056	0.045*	<0.001***	0.01*
	Orbital part of inferior frontal gyrus	<0.001***	0.664	0.019*	<0.001***	<0.001***	0.016*	0.005**	<0.001***	<0.001***	0.219	<0.001***	0.002**	0.51	0.012*	0.046*	<0.001***	0.111	0.48	<0.001***	0.058	0.034*	<0.001***	0.004**	0.065
	Triangular part of inferior frontal gyrus	<0.001***	0.454	<0.001***	<0.001***	<0.001***	<0.001***	<0.001***	0.001**	<0.001***	<0.001***	0.02*	0.001**	0.083	<0.001***	0.179	<0.001***	<0.001***	0.781	0.033*	0.019*	0.054	<0.001***	<0.001***	<0.001***
	Frontal operculum	<0.001***	<0.001***	<0.001***	<0.001***	<0.001***	<0.001***	<0.001***	<0.001***	<0.001***	<0.001***	0.021*	<0.001***	0.008**	<0.001***	0.263	<0.001***	<0.001***	<0.001***	<0.001***	<0.001***	<0.001***	<0.001***	<0.001***	<0.001***
	Gyrus rectus and orbital gyri	<0.001***	0.918	0.067	<0.001***	0.005**	<0.001***	<0.001***	0.082	<0.001***	0.023*	0.056	<0.001***	0.131	0.835	0.623	<0.001***	<0.001***	0.019*	0.096	0.979	0.201	<0.001***	0.008**	0.325
	Medial frontal cortex	<0.001***	0.46	0.003**	<0.001***	0.223	0.006**	0.001**	0.104	<0.001***	0.037*	0.023*	<0.001***	0.023*	0.883	0.338	<0.001***	0.07	0.987	<0.001***	<0.001***	0.177	<0.001***	0.278	0.002**
	Supplementary motor cortex	0.021*	0.855	0.002**	0.071	0.289	0.13	0.035*	0.048*	0.694	0.051	0.041*	0.51	0.296	0.015*	0.068	0.072	0.287	0.427	0.026*	0.417	0.034*	0.636	<0.001***	0.001**
	Anterior cingulate	<0.001***	0.395	<0.001***	<0.001***	<0.001***	0.009**	0.001**	0.094	0.003**	0.032*	0.205	0.002**	0.839	0.002**	0.69	<0.001***	0.007**	0.01*	<0.001***	<0.001***	0.017*	0.012*	<0.001***	<0.001***
	Middle cingulate	0.198	0.035*	<0.001***	0.197	0.214	0.021*	0.191	0.926	0.976	0.464	0.69	0.86	0.957	0.755	0.511	0.083	0.637	0.499	0.023*	0.8	0.952	0.779	0.007**	0.017*
Temporal	Superior temporal gyrus	<0.001***	0.032*	0.156	0.384	0.267	0.057	0.004**	0.121	0.075	0.617	0.031*	0.148	0.623	0.008**	0.312	0.093	0.617	0.728	0.163	<0.001***	0.01*	0.006**	0.076	0.203
	Middle temporal gyrus	<0.001***	0.03*	0.018*	<0.001***	0.003**	<0.001***	<0.001***	<0.001***	<0.001***	<0.001***	<0.001***	0.012*	0.02*	<0.001***	0.612	0.562	<0.001***	0.464	<0.001***	<0.001***	<0.001***	<0.001***	0.323	0.069
	Inferior temporal gyrus	<0.001***	<0.001***	<0.001***	<0.001***	<0.001***	<0.001***	<0.001***	<0.001***	<0.001***	<0.001***	<0.001***	0.002**	0.835	<0.001***	0.704	<0.001***	0.413	0.126	<0.001***	<0.001***	0.181	<0.001***	0.479	<0.001***
	Planum temporale	0.038*	<0.001***	0.264	0.086	0.004**	0.035*	<0.001***	0.348	0.332	<0.001***	0.004**	0.901	<0.001***	0.063	0.411	0.332	0.642	0.033*	0.009**	0.109	0.03*	<0.001***	<0.001***	0.024*
	Transverse temporal gyrus	<0.001***	0.093	<0.001***	<0.001***	0.717	<0.001***	<0.001***	<0.001***	<0.001***	<0.001***	<0.001***	0.015*	<0.001***	<0.001***	0.029*	<0.001***	0.089	0.074	<0.001***	<0.001***	0.002**	0.395	<0.001***	<0.001***
	Fusiform and parahippocampal gyri	<0.001***	0.01*	0.058	0.003**	0.001**	0.06	0.02*	<0.001***	0.002**	0.004**	<0.001***	0.49	0.087	0.003**	0.61	0.24	0.341	0.664	0.458	0.216	0.751	0.009**	0.011*	0.025*
	Hippocampus	0.331	0.134	0.976	0.079	0.02*	0.071	<0.001***	0.206	0.001**	0.051	0.541	<0.001***	0.343	0.487	0.019*	0.974	0.164	0.256	0.972	0.348	0.245	0.63	0.003**	0.567
	Amygdala	<0.001***	0.212	0.395	0.004**	0.174	0.008**	0.013*	0.926	0.014*	<0.001***	0.27	0.039*	0.894	0.242	0.48	0.41	0.404	0.617	0.44	0.163	0.446	0.049*	0.042*	0.514
Insula	Anterior insula	<0.001***	0.057	0.004**	<0.001***	0.067	0.212	0.008**	0.009**	0.377	0.019*	0.006**	0.384	0.037*	<0.001***	0.332	0.005**	0.622	0.523	0.007**	0.177	0.266	0.665	<0.001***	<0.001***
	Posterior insula	<0.001***	0.971	<0.001***	<0.001***	0.099	<0.001***	<0.001***	<0.001***	<0.001***	<0.001***	<0.001***	0.113	0.389	0.559	0.184	0.083	0.202	0.839	<0.001***	<0.001***	<0.001***	0.173	<0.001***	<0.001***
Parietal	Parietal operculum	0.744	<0.001***	<0.001***	0.788	0.883	0.077	<0.001***	0.046*	0.058	<0.001***	0.037*	0.004**	<0.001***	<0.001***	0.107	<0.001***	0.001**	<0.001***	0.003**	0.011*	0.163	<0.001***	<0.001***	<0.001***
	Supramarginal gyrus	<0.001***	0.02*	0.009**	<0.001***	0.141	0.004**	<0.001***	<0.001***	0.546	<0.001***	0.001**	0.058	0.127	<0.001***	0.827	<0.001***	<0.001***	0.048*	<0.001***	<0.001***	0.562	0.003**	<0.001***	0.021*
	Angular gyrus	<0.001***	0.16	<0.001***	<0.001***	<0.001***	<0.001***	<0.001***	<0.001***	<0.001***	<0.001***	<0.001***	<0.001***	<0.001***	<0.001***	0.776	<0.001***	0.006**	0.035*	<0.001***	<0.001***	0.004**	<0.001***	<0.001***	<0.001***
	Precuneus	<0.001***	0.032*	<0.001***	<0.001***	0.603	0.006**	<0.001***	<0.001***	0.929	<0.001***	0.935	0.143	0.003**	<0.001***	0.185	0.03*	0.366	0.454	0.06	<0.001***	0.093	0.067	<0.001***	<0.001***
	Posterior cingulate	<0.001***	0.807	0.01*	<0.001***	<0.001***	0.143	<0.001***	<0.001***	0.006**	<0.001***	0.046*	<0.001***	<0.001***	<0.001***	0.84	0.008**	0.075	0.135	0.031*	0.503	0.637	<0.001***	<0.001***	0.012*
Occipital	Cuneus	<0.001***	<0.001***	<0.001***	0.565	<0.001***	<0.001***	<0.001***	0.079	0.081	<0.001***	0.193	0.018*	0.071	0.003**	0.708	<0.001***	0.115	0.095	<0.001***	<0.001***	0.017*	0.043*	<0.001***	0.01*
	Inferior occipital gyrus and occipital pole	<0.001***	<0.001***	0.303	<0.001***	<0.001***	0.826	<0.001***	<0.001***	0.248	<0.001***	<0.001***	0.865	0.008**	<0.001***	0.779	<0.001***	0.055	0.005**	<0.001***	0.622	0.03*	0.003**	<0.001***	0.001**

The table shows the *p* values of delta, theta, alpha, sigma, beta, gamma, HF power, and wake-related ratio during arousal onset, body, and offset of SW arousals, relative to baseline. The first row shows the scalp-EEG activity and the rest shows the SEEG activity in each region. *p* values < 0.001 are marked with ***; $0.001 \leq p < 0.01$ are marked with **; $0.01 \leq p < 0.05$ are marked with *.

N/A, not applicable.

Table 3. *p* values of scalp-EEG and SEEG activities during non-SW arousals relative to baseline

		Delta (0.5–4 Hz)			Theta (4–8 Hz)			Alpha (8–13 Hz)			Sigma (10–16 Hz)			Beta (17–30 Hz)			Gamma (30–80 Hz)			High frequency (80–250 Hz)			Wake-related ratio		
		Onset	Body	Offset	Onset	Body	Offset	Onset	Body	Offset	Onset	Body	Offset	Onset	Body	Offset	Onset	Body	Offset	Onset	Body	Offset	Onset	Body	Offset
Scalp	Scalp-EEG	<0.001***	0.016*	<0.001***	0.436	0.395	<0.001***	<0.001***	0.261	<0.001***	<0.001***	0.485	<0.001***	<0.001***	<0.001***	0.928	N/A	N/A	N/A	N/A	N/A	N/A	0.947	<0.001***	<0.001***
Frontal	Middle frontal gyrus	0.014*	<0.001***	<0.001***	0.142	0.323	0.005**	<0.001***	0.724	0.019*	<0.001***	0.149	0.043*	0.002**	<0.001***	0.716	0.002**	0.554	0.475	0.006**	0.001**	0.684	0.505	<0.001***	<0.001***
	Orbital part of inferior frontal gyrus	0.007**	0.038*	<0.001***	0.167	0.185	<0.001***	0.175	0.001**	0.004**	0.956	0.014*	0.019*	0.001**	0.209	0.016*	0.001**	0.111	0.814	0.054	0.485	0.524	0.338	<0.001***	0.076
	Triangular part of inferior frontal gyrus	0.159	0.035*	<0.001***	0.007**	0.263	0.019*	0.018*	0.415	<0.001***	0.034*	0.424	<0.001***	0.087	0.023*	0.704	0.002**	0.098	0.696	0.53	0.116	0.209	0.112	0.003**	0.005**
	Frontal operculum	<0.001***	<0.001***	<0.001***	<0.001***	0.386	<0.001***	<0.001***	0.518	0.002**	0.07	0.222	0.01*	0.606	<0.001***	0.472	<0.001***	<0.001***	0.791	<0.001***	0.54	0.681	0.18	<0.001***	<0.001***
	Gyrus rectus and orbital gyri	<0.001***	0.007**	<0.001***	<0.001***	0.784	<0.001***	0.001**	0.666	<0.001***	0.198	0.811	<0.001***	0.019*	0.498	0.772	<0.001***	<0.001***	0.699	0.293	0.492	0.007**	0.402	<0.001***	0.064
	Medial frontal cortex	<0.001***	0.041*	<0.001***	0.056	0.823	0.002**	0.142	<0.001***	0.006**	0.79	<0.001***	0.023*	0.018*	0.664	0.24	0.008**	0.21	0.622	0.029*	0.086	0.186	0.029*	<0.001***	<0.001***
	Supplementary motor cortex	0.005**	0.66	0.013*	0.001**	0.023*	0.003**	<0.001***	<0.001***	0.008**	<0.001***	0.003**	0.005**	<0.001***	<0.001***	0.894	0.132	0.682	0.617	0.413	0.819	0.446	0.01**	<0.001***	0.071
	Anterior cingulate	<0.001***	0.015*	<0.001***	0.014*	0.32	<0.001***	<0.001***	0.004**	<0.001***	0.004**	0.224	<0.001***	0.503	0.055	0.012*	<0.001***	0.996	0.716	<0.001***	0.668	0.681	0.338	<0.001***	0.026*
	Middle cingulate	0.072	<0.001***	<0.001***	0.766	0.022*	0.003**	0.23	0.704	0.002**	0.66	0.438	0.004**	0.128	0.006**	0.434	0.027*	0.53	0.245	0.005**	0.038*	0.676	<0.001***	<0.001***	0.206
Temporal	Superior temporal gyrus	0.093	0.004**	0.008**	0.971	0.425	0.088	0.495	0.458	0.371	0.263	0.344	0.341	0.263	0.005**	0.675	0.98	0.197	0.905	0.252	0.708	0.958	<0.001***	<0.001***	<0.001***
	Middle temporal gyrus	0.28	0.047*	0.026*	0.461	0.173	0.005**	0.044*	0.441	0.005**	0.08	0.335	0.021*	0.185	0.028*	0.612	0.425	0.428	0.639	0.348	0.356	0.971	0.229	0.005**	0.049*
	Inferior temporal gyrus	0.114	0.154	0.004**	0.004**	0.425	<0.001***	0.033*	0.366	0.004**	0.001**	0.697	0.013*	<0.001***	0.001**	0.53	0.056	0.623	0.264	0.427	0.656	0.658	0.425	0.034*	0.008**
	Transverse temporal gyrus	0.154	<0.001***	0.155	0.459	0.132	0.034*	0.014*	0.978	0.175	0.001**	0.036*	0.017*	0.021*	0.467	0.672	0.165	0.088	0.139	0.011*	<0.001***	0.026*	<0.001***	<0.001***	0.107
	Fusiform and parahippocampal gyri	<0.001***	0.053	<0.001***	0.077	0.86	0.006**	<0.001***	0.029*	0.035*	<0.001***	0.143	0.088	0.155	0.458	0.906	<0.001***	0.052	0.154	0.059	0.234	0.759	0.122	<0.001***	<0.001***
	Hippocampus	0.443	0.017*	0.105	<0.001***	0.001**	<0.001***	0.206	0.475	0.003**	0.395	0.766	0.004**	0.853	0.105	0.287	0.143	0.686	0.142	0.341	0.328	0.01*	0.647	0.008**	0.834
	Amygdala	0.447	0.151	0.197	0.511	0.031*	0.191	0.976	0.478	0.032*	0.647	0.281	0.132	0.355	0.707	0.971	0.448	0.759	0.338	0.356	0.262	0.529	0.502	0.314	0.496
Insula	Anterior insula	0.024*	0.267	0.899	<0.001***	0.031*	0.263	0.001**	0.005**	0.976	<0.001***	<0.001***	0.137	<0.001***	<0.001***	0.897	0.623	0.025*	0.367	<0.001***	0.756	0.286	0.15	0.01*	0.727
	Posterior insula	0.046*	0.012*	0.04*	0.407	0.846	0.045*	0.173	0.693	0.022*	0.546	0.987	0.01**	0.203	0.077	0.903	0.057	0.378	0.301	0.317	0.343	0.034*	<0.001***	<0.001***	0.135
Parietal	Parietal operculum	0.001**	<0.001***	0.001**	0.015*	0.16	<0.001***	0.056	0.546	0.027*	0.002**	0.046*	0.293	<0.001***	<0.001***	0.796	0.482	0.114	0.005**	0.267	0.048*	0.009**	<0.001***	<0.001***	0.007**
	Supramarginal gyrus	0.141	0.047*	0.021*	0.395	0.018*	0.013*	0.124	0.61	0.007**	0.18	0.935	0.023*	<0.001***	0.049*	0.776	0.152	0.015*	0.947	<0.001***	<0.001***	0.001**	0.045*	0.002**	0.006**
	Angular gyrus	0.01*	<0.001***	<0.001***	<0.001***	0.013*	<0.001***	<0.001***	<0.001***	<0.001***	<0.001***	<0.001***	<0.001***	<0.001***	<0.001***	0.652	0.229	0.811	0.856	<0.001***	0.491	0.536	<0.001***	<0.001***	<0.001***
	Precuneus	0.007**	<0.001***	<0.001***	0.561	0.005**	<0.001***	0.012*	0.003**	<0.001***	0.009**	0.017*	<0.001***	<0.001***	<0.001***	0.114	0.445	0.009**	0.445	<0.001***	<0.001***	0.014*	<0.001***	<0.001***	<0.001***
	Posterior cingulate	0.39	0.043*	0.038*	0.883	0.224	<0.001***	0.004**	0.507	0.013*	<0.001***	0.407	0.004**	<0.001***	<0.001***	0.138	0.312	0.424	0.987	0.357	0.667	0.447	0.002**	0.004**	0.113
Occipital	Cuneus	0.033*	<0.001***	<0.001***	0.057	<0.001***	<0.001***	0.019*	0.011*	<0.001***	0.036*	0.082	<0.001***	0.034*	<0.001***	0.945	<0.001***	0.009**	0.666	<0.001***	<0.001***	0.056	<0.001***	<0.001***	<0.001***
	Inferior occipital gyrus and occipital pole	<0.001***	0.118	<0.001***	<0.001***	<0.001***	<0.001***	<0.001***	<0.001***	<0.001***	<0.001***	<0.001***	<0.001***	<0.001***	<0.001***	0.641	<0.001***	<0.001***	0.542	0.346	0.001**	0.416	<0.001***	<0.001***	<0.001***

The table shows the *p* values of delta, theta, alpha, sigma, beta, gamma, HF power, and wake-related ratio during arousal onset, body, and offset of non-SW arousals, relative to baseline. The first row shows the scalp-EEG activity and the rest shows the SEEG activity in each region. *p* values < 0.001 are marked with ***; $0.001 \leq p < 0.01$ are marked with **; $0.01 \leq p < 0.05$ are marked with *.
N/A, not applicable.

Table 4. Comparisons of scalp-EEG and SEEG activities between SW and non-SW arousals

		Delta (0.5–4 Hz)			Theta (4–8 Hz)			Alpha (8–13 Hz)			Sigma (10–16 Hz)			Beta (17–30 Hz)			Gamma (30–80 Hz)			High frequency (80–250 Hz)			Wake-related ratio		
		Onset	Body	Offset	Onset	Body	Offset	Onset	Body	Offset	Onset	Body	Offset	Onset	Body	Offset	Onset	Body	Offset	Onset	Body	Offset	Onset	Body	Offset
Scalp	Scalp-EEG	0.144*	0.132*	0.092	0.24***	0.157*	0.076	0.105	0.062	0.077	0.032	0.013	0.061	0.078	0.124*	0.173**	N/A	N/A	N/A	N/A	N/A	N/A	−0.098	−0.058	−0.019
Frontal	Middle frontal gyrus	0.121	0.161*	0.087	0.067	0.11	0.083	0.023	0.038	0.145	0.056	0.057	0.116	−0.13	−0.065	0.136	−0.069	−0.131	0.023	−0.102	−0.04	−0.062	−0.15*	−0.192*	−0.038
	Orbital part of inferior frontal gyrus	0.197*	0.164	0.11	0.147	0.132	0.134	0.035	0.049	0.056	0.054	0.085	0.047	0.18	0.054	0.038	0.041	0.041	−0.006	0.036	−0.008	−0.015	−0.15	−0.089	−0.049
	Triangular part of inferior frontal gyrus	0.241**	0.187	0.125	0.226*	0.233**	0.077	−0.056	0.005	0.18*	−0.068	−0.012	0.202	−0.051	−0.086	0.001	−0.046	−0.022	−0.045	−0.03	−0.012	−0.011	−0.258**	−0.167	−0.034
	Frontal operculum	0.157*	0.087	0.069	0.081	0.064	0.081	0.073	0.132*	0.064	0.016	0.068	0.05	−0.076	−0.001	0.07	−0.098	−0.039	−0.108	−0.176*	−0.068	−0.076	−0.141*	0.001	−0.02
	Gyrus rectus and orbital gyri	0.083	0.119*	0.089	0.075	0.094	0.134**	−0.062	0.032	0.126*	−0.014	0.046	0.134*	0.049	−0.018	−0.028	0.081	0.012	−0.086	−0.007	0.042	−0.146*	−0.123**	−0.099*	−0.042
	Medial frontal cortex	−0.104	0.258*	0.384*	−0.072	0.082	0.359*	−0.069	−0.341*	0.361	0.107	−0.399**	0.297	0.292	−0.056	0.2	0.25	0.115	−0.062	0.26	0.211	0.171	0.033	−0.415**	−0.318*
	Supplementary motor cortex	0.363	−0.012	−0.386*	0.263	0.133	0.051	0.267	0.297	0.141	0.202	0.307	0.295	0.08	0.337	0.335	−0.151	0.085	−0.035	−0.336	−0.139	−0.411	−0.198	0.477**	0.481*
	Anterior cingulate	0.008	0.146*	0.078	0.001	0.011	0.202***	−0.128	−0.132	0.144*	−0.103	−0.053	0.164**	0.039	−0.037	0.148	0.097	−0.031	0.001	0.108	−0.006	0.013	−0.1*	−0.229***	0.01
	Middle cingulate	0.758	−1.003	−1.845**	0.725	−0.595	−1.162*	0.723	0.068	0.089	0.397	−0.217	0.168	−0.075	−0.256	0.384	−0.706	−0.155	−0.169	−1.226	−0.122	0.049	0.055	1.17*	1.304*
Temporal	Superior temporal gyrus	0.278**	0.495**	0.404*	0.041	0.129	0.205	−0.032	−0.017	0.072	−0.088	−0.025	0.079	−0.153	−0.274	0.014	−0.056	−0.203	−0.032	−0.163	0.029	0.043	−0.383***	−0.722***	−0.522**
	Middle temporal gyrus	−0.123	0.475*	0.435	−0.076	0.358	0.483*	−0.431	0.238	0.576*	−0.357	0.309	0.493	−0.315	−0.382	−0.124	−0.204	−0.173	−0.097	−0.219	−0.187	0.133	−0.31	−0.555*	−0.363
	Inferior temporal gyrus	0.031	0.299	0.494*	−0.238	0.222	0.734***	−0.307	0.227	0.481*	−0.307	0.136	0.421	−0.401**	−0.423*	0.086	0.105	−0.043	−0.22	−0.228	−0.038	−0.071	−0.301	−0.367*	−0.429*
	Transverse temporal gyrus	0.37*	0.438**	0.127	0.24	0.236	0.205	−0.167	0.105	0.142	−0.24	−0.144	0.321	−0.243	−0.019	−0.015	0.035	0.18	0.139	0.181	0.383*	0.191	−0.474**	−0.414**	−0.127
	Fusiform and parahippocampal gyri	−0.195*	0.176*	0.259**	−0.067	0.069	0.263*	−0.13*	−0.096	0.177	−0.189*	−0.033	0.167	−0.076	−0.004	0.02	0.173**	0.146	0.15	−0.215	−0.122	0.04	0.075	−0.373***	−0.252***
	Hippocampus	0.174	0.299	0.246	0.61**	0.424*	0.677***	0.35	0.175	0.302	0.229	−0.029	0.327	0.017	−0.279	0.088	0.188	0.022	0.134	0.144	0.111	0.241	−0.047	−0.322	−0.054
	Amygdala	0.654	0.778	0.713	0.501	1.302	0.655	0.102	0.384	1.222	0.437	0.661	0.771	0.545	−0.278	0.014	0.419	−0.225	−0.548	0.579	−0.721	0.406	−0.445	−0.448	−0.344
Insula	Anterior insula	0.047	0.009	−0.077	−0.006	−0.008	0.042	−0.021	0.012	−0.059	−0.028	0.072	0.043	−0.097	−0.021	0.062	−0.214*	−0.094	−0.043	−0.107	−0.083	−0.01	−0.106	0.007	0.07
	Posterior insula	0.472*	0.514*	0.307	−0.155	0.062	0.331	−0.19	−0.024	0.462	−0.015	0.063	0.535*	0.268	−0.376	0.038	0.405	0.188	−0.231	0.263	−0.045	−0.366	−0.738***	−0.657**	−0.17
Parietal	Parietal operculum	0.334**	0.348**	0.147	0.296*	0.155	0.387**	−0.111	−0.025	0.196	−0.2	−0.168	0.057	−0.409**	−0.393**	−0.016	−0.174	0.068	0.141	0.041	0.151	0.183	−0.425***	−0.427***	−0.071
	Supramarginal gyrus	0.404***	0.117	0.103	0.319***	0.229*	0.11	0.054	0.158	0.111	0.042	0.103	0.099	−0.138	−0.049	−0.032	−0.164	−0.317***	−0.119	−0.168	−0.01	0.047	−0.237**	−0.102	−0.057
	Angular gyrus	0.114*	0.242***	0.357***	−0.001	0.008	0.417***	−0.174*	−0.136*	0.37***	−0.231**	−0.171*	0.41***	−0.413***	−0.246***	0.033	−0.084	−0.069	−0.025	0.087	0.005	0.005	−0.366***	−0.411***	−0.26***
	Precuneus	0.38***	0.188**	0.07	0.234***	0.06	0.116*	0.108	−0.04	0.129*	0.057	−0.086	0.108	−0.093	−0.128*	0.1	−0.108	−0.116	−0.008	0.023	0.056	−0.004	−0.317***	−0.266***	−0.004
	Posterior cingulate	0.39***	0.193*	0.137	0.263**	0.2*	0.274**	0.015	0.139	0.143	0.065	0.116	0.121	−0.185	−0.167	−0.119	−0.06	−0.029	−0.04	−0.012	0.059	0.061	−0.349***	−0.189*	−0.098
Occipital	Cuneus	0.489***	−0.181*	−0.253*	0.114	−0.189	−0.309**	0.304*	0.087	−0.06	0.266*	0.073	−0.087	0.06	0.154	−0.038	−0.237*	−0.058	−0.123	−0.44***	−0.182	−0.145	−0.302**	0.205*	0.178
	Inferior occipital gyrus and occipital pole	−0.068	0.187*	0.397***	−0.307***	−0.119	0.222**	−0.299***	−0.3***	0.238**	−0.217***	−0.209**	0.283***	−0.131*	−0.297***	0.043	0.273***	0.199**	−0.007	−0.178	−0.094	−0.106	−0.28***	−0.538***	−0.411***

The table shows the effect size (Cohen's *d*) of the direct comparisons of delta, theta, alpha, sigma, beta, gamma, HF power, and wake-related ratio during arousal onset, body, and offset between SW and non-SW arousals. The first row shows the scalp-EEG activity and the rest shows the SEEG activity in each region. Comparisons with p values <0.001 are marked with *** after the effect size; the ones with $0.001 \leq p < 0.01$ are marked with **; and the ones with $0.01 \leq p < 0.05$ are marked with *. To help interpret the positive and negative signs of the effect size: If the band power increases during both arousal types, a positive effect size means the increase during SW arousals is stronger; if the power decreases during both arousal types, a positive effect size means the decrease during SW arousals is weaker; and if the band power increases during SW arousals and decreases during non-SW arousals, the effect size (with $p < 0.05$) will be positive.
N/A, not applicable.

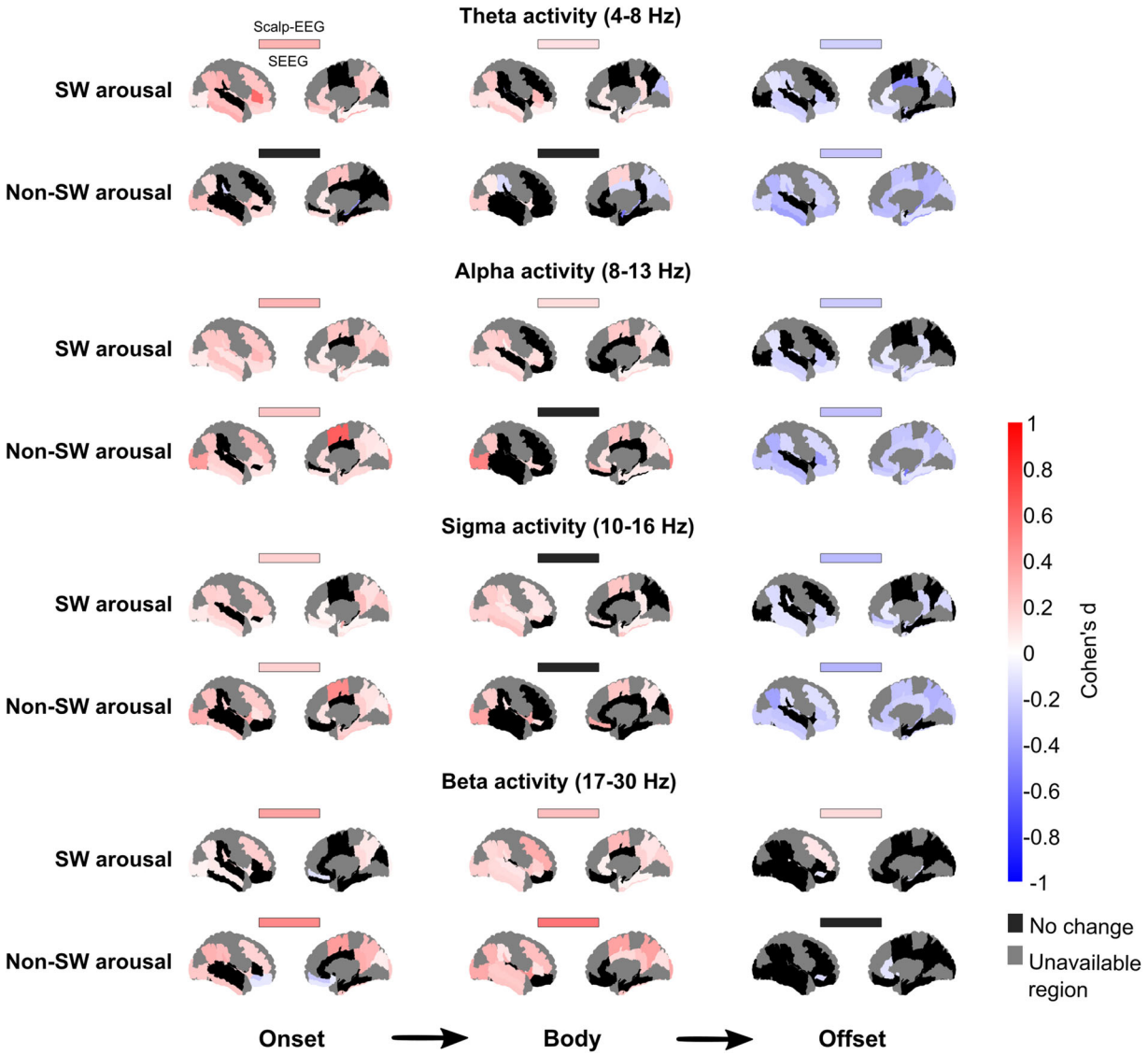

Figure 5. Theta, alpha, sigma, and beta activities increase in many regions during the two arousal types. The color represents the effect size of the change in theta, alpha, sigma, and beta band power relative to baseline on the scalp-EEG (bar) and SEEG (brain visualizations) during the arousal onset, body, and offset of SW and non-SW arousals. Red represents an increase in the band power, while blue represents a decrease in band power. Regions that were available in <3 patients are marked in gray, and regions with no significant change in band power are in black. We observed that many regions showed an increase in theta, alpha, sigma, and beta activities during two types of arousals which turned to a decrease or returned to baseline afterward.

Intracranial EEG signature across the different arousal types

Across all arousal types, theta, alpha, sigma, and beta activities increased in up to 25 regions. No previous studies investigated activity patterns during different arousal types, but our result is consistent with previous findings in frontoparietal regions during spontaneous and nociceptive-induced NREM arousals (Nobili et al., 2011; Peter-Derex et al., 2015; Ruby et al., 2021). It also aligns with previous results in fronto-temporo-parietal regions during confusional arousals, a NREM parasomnia (Flamand et al., 2018). Scalp-EEG findings showed as well that the occipital alpha power increases during behavioral arousals (Setzer et al., 2022). We proposed that the widespread theta to beta increase indicates a higher vigilance state during all arousal types, because these frequency bands have been suggested as wake-related (Berger, 1929; Jasper and Penfield, 1949; Buzsáki, 2011; Adamantidis et al., 2019).

We also found that gamma and HF activities decreased in up to 18 regions across the five brain lobes. In the only study that explored activities in frequency range >30 Hz during arousals, gamma power decreased in the hippocampus and increased in the prefrontal cortex (Ruby et al., 2021), which is different from our results of no change in the hippocampus and a decrease in frontal regions. This discrepancy may result from the different durations between arousals and awakenings which were also analyzed in their study. Compared with NREM sleep, activities >30 Hz has higher power during wakefulness in the fronto-temporo-occipital regions (Cantero et al., 2004; Mikulan et al., 2018). This is consistent with our HF increase in the temporal lobe but contrasts with our HF decrease in other regions and the widespread gamma decrease. Given that the intracranial increase of >30 Hz activity across four lobes was associated with memory processing and cognitive tasks (Burke et al., 2014; Kucewicz et al., 2014; Greenberg et al., 2015; Lundqvist et al., 2016; Castelhano et al., 2017; Dickey et al., 2022; Liu et al., 2022), the widespread gamma and HF decrease may explain the absence of awareness and recollection during arousals.

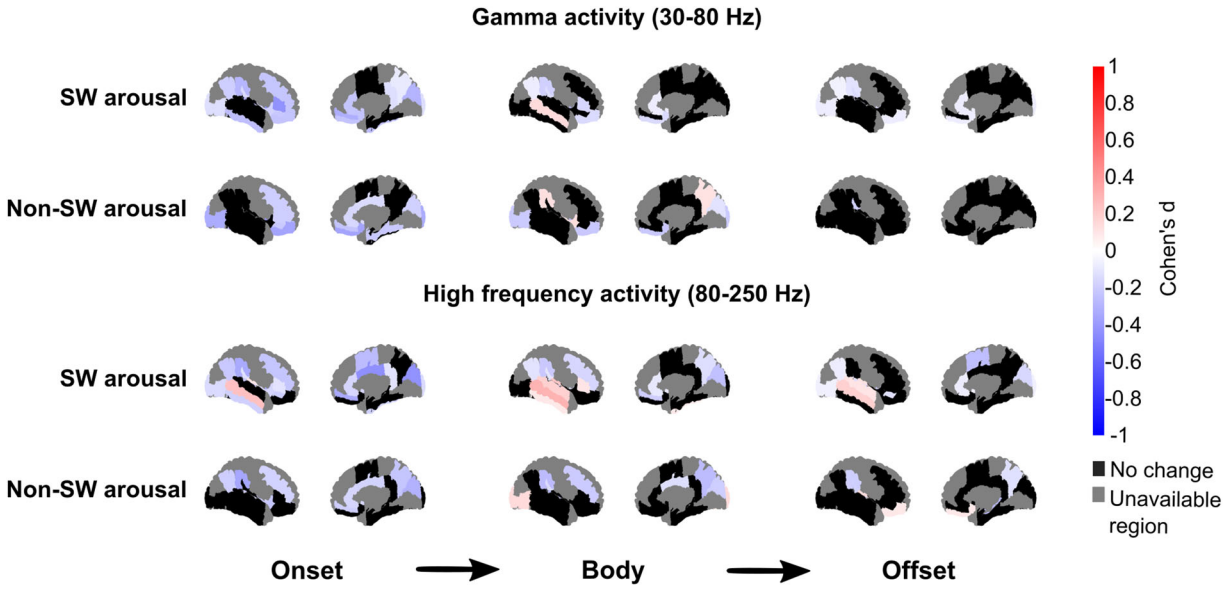

Figure 6. Gamma and HF activities decrease in many regions during the two arousal types. The color represents the effect size of the change in gamma and HF band power relative to baseline on the scalp-EEG (bar) and SEEG (brain visualizations) during the arousal onset, body, and offset of SW and non-SW arousals. Red represents an increase in the band power while blue represents a decrease in band power. Regions that were available in <3 patients are marked in gray, and regions with no significant change in band power are in black. We observed that many regions showed a decrease in gamma and HF activities during two types of arousals which continued to decrease or returned to baseline afterward.

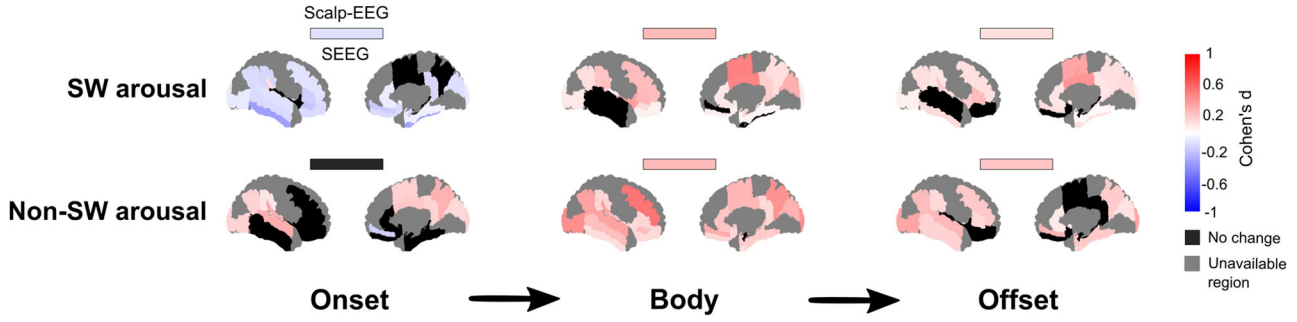

Figure 7. SW arousals show sleep-related properties during the onset, while non-SW arousals are wake-related throughout. The color represents the effect size of the wake-related properties on the scalp-EEG (bar) and SEEG (brain visualizations) during the arousal onset, body, and offset of SW and non-SW arousals. Red represents a stronger activity change in the theta, alpha, and beta frequency range than delta, while blue represents the opposite. Regions that were available in <3 patients are marked in gray, and regions with no significant change in band power are in black. We observed that sleep-related responses occurred during the onset of SW arousals, while wake-related responses persisted throughout non-SW arousals. We also observed coexistence of sleep-related and wake-related regions during the onset of SW and non-SW arousals.

Differences across the various arousal types

The two arousal types showed distinct intracranial delta activities and wake-related properties. SW arousals showed a widespread delta increase and sleep-related properties during onset, while non-SW arousals showed a widespread delta decrease and wake-related properties. The early sleep-related properties of SW arousals may reflect their sleep-preserving properties. This result also confirms our hypothesis that non-SW arousals represent a higher level of cortical activation than SW arousals which may indicate a higher probability of awakening. While we initially hypothesized that "slow" arousals are more likely to occur during the first half of the night when the sleep homeostatic pressure is high, the result suggests that the occurrence of SW and non-SW arousals may not be heavily influenced by sleep homeostatic pressure.

Interestingly, we further observed a simultaneous increase in delta (associated with sleep) and theta, alpha, beta (associated with wakefulness) activities in over 20 regions during SW arousals. This is a significant finding because the paradoxical coexistence of these activities was also reported in frontoparietal regions during confusional arousals, a type of NREM parasomnia when individuals present wake-like behavior without memory or awareness (Mahowald and Schenck, 2005; Terzaghi et al., 2009). Notably, a recent study showed that the scalp-EEG activity does not differ between arousal periods with simple and complex movements (Mainieri et al., 2022). Therefore, the intracranial activity pattern of SW arousals might help us understand the pathology underlying NREM parasomnias. Future studies are needed to investigate the temporal dynamics of two arousal types and how SW arousals may be prolonged to and associated with abnormal behaviors in parasomnias.

Intracranial activity after sleep arousals

During the postarousal offset, delta, theta, alpha, and sigma activities widely decreased compared with baseline, while beta, gamma, and HF activities returned to baseline in many regions.

This aligns with previous scalp-EEG findings in the delta, theta, sigma, alpha, and beta band power (Bruce et al., 2011). Since sleep depth—defined as the difficulty to wake up—positively correlates with delta power assessed on scalp-EEG (Neckelmann and Ursin, 1993; Berry et al., 1998; Younes et al., 2020), our results indicate that many regions showed lighter sleep immediately after arousals than prearousal periods. This effect is important, since during sleep disorders associated with sleep fragmentation such as obstructive sleep apnea, arousals may not only disrupt brain activity during sleep but also lighten sleep and facilitate further arousals, which were known to occur more frequently as sleep depth decreases (Terzano et al., 2000, 2002, 2005, Nobili et al., 2011). We wish to distinguish the sleep depth here from the subjectively perceived sleep depth, which was recently shown to decouple with delta power (Stephan et al., 2021).

Spatial heterogeneity of sleep arousals

We reported a heterogeneous activity across brain regions during sleep arousals, which aligns with previous research (Peter-Derex et al., 2015). These results showed that, despite having a common intracranial signature, sleep arousals have local properties that support the notion that sleep is a locally regulated phenomenon (Huber et al., 2004; Krueger et al., 2008; Ferrara and De Gennaro, 2011). The local properties of sleep were also reported for other sleep oscillations such as spindles, K-complexes, and sawtooth waves (Frauscher et al., 2015a, 2020; Latreille et al., 2020). Among all the regions that showed unique activities, the following four are of particular interest. First, the middle cingulate cortex exhibiting no increase in theta to beta activity during SW arousals aligns with what was observed during confusional arousals (Flamand et al., 2018). This structure was found to link to affective, motor, and somatosensory networks in humans (Oane et al., 2020). Second, the hippocampus showing no increases in delta power during both arousal types is in line with previous research during physiological and confusional arousals (Flamand et al., 2018; Ruby et al., 2021). Third, the parietal operculum, which showed a delta decrease during both arousal types, contains the secondary somatosensory cortex (Meyer et al., 2016). Lastly, the gamma and HF increase in the superior and middle temporal gyrus during SW arousals was associated with auditory attention and language tasks (Thampratankul et al., 2010; Nelson et al., 2017; Nourski et al., 2017; Omigie et al., 2019). The delta decrease in the parietal operculum and HF increase in the temporal lobe might allow the brain to process important somatosensory and auditory information from the environment, since arousals could be induced by nociceptive and auditory stimulation.

Strengths and potential limitations

This work represents the first intracranial study of different types of NREM sleep arousals. Our dataset is currently the largest intracranial dataset of sleep arousals with a wide brain coverage in humans. Using a wide frequency band analysis, we identified the intracranial signatures of arousals without a priori hypotheses, especially in the HF range (80–250 Hz) that remained unexplored in past works. Additionally, our registration of channel positions to a common stereotaxic space allowed us to include channels with physiological activity from all patients. These strengths allowed us to provide a comprehensive description of the local brain activities across both arousal types.

Our dataset did not contain autonomic or behavioral measures, which would expand the picture of physiological activation during arousals. We also acknowledge the potential limitation of using data from patients with epilepsy, the only group where prolonged intracranial recordings are performed. However, we selected channels with physiological activity and excluded nights with electroclinical seizures. Although antiseizure medication might modify sleep architecture (Jain and Glauser, 2013; Shvarts and Chung, 2013), the scalp-EEG features of our included arousals were similar to those observed in healthy subjects (Bonnet and Arand, 2007; Azarbarzin et al., 2014). It could be interesting to explore in future work the aperiodic component that was recently shown to differ among the various states of vigilance and see if there are changes in the background preceding SW and non-SW arousals (Donoghue et al., 2020; Lendner et al., 2020).

In conclusion, while SW and non-SW arousals correspond to different levels of brain activation, they both reflect a heightened vigilance state with the decrease in HFs potentially explaining the absence of awareness and recollection of these events. SW arousals notably present similar intracranial patterns to NREM parasomnias and could potentially help us understand the underlying pathology.

References

Adamantidis AR, Gutierrez Herrera C, Gent TC (2019) Oscillating circuitries in the sleeping brain. Nat Rev Neurosci 20:746–762.

ASDA (1992) EEG arousals: scoring rules and examples: a preliminary report from the Sleep Disorders Atlas Task Force of the American Sleep Disorders Association. Sleep 15:173–184.

Azarbarzin A, Ostrowski M, Hanly P, Younes M (2014) Relationship between arousal intensity and heart rate response to arousal. Sleep 37:645–653.

Berger H (1929) Über das Elektrenkephalogramm des Menschen. Arch Psychiatr Nervenkr 87:527–570.

Berry RB, Asyali MA, McNellis MI, Khoo MCK (1998) Within-night variation in respiratory effort preceding apnea termination and EEG delta power in sleep apnea. J Appl Physiol 85:1434–1441.

Berry RB, Quan SF, Abreu AR, Bibbs ML, DelRosso L, Harding SM, Mao M-M, Plante DT, Pressman MR, Troester MM (2020) *The AASM manual for the scoring of sleep and associated events: rules, terminology and technical specifications*. Darien, Ilinois: American Academy of Sleep Medicine.

Bonnet MH, Arand DL (2007) EEG arousal norms by age. J Clin Sleep Med 3: 271–274.

Boselli M, Parrino L, Smerieri A, Terzano MG (1998) Effect of age on EEG arousals in normal sleep. Sleep 21:351–357.

Bruce EN, Bruce MC, Ramanand P, Hayes D (2011) Progressive changes in cortical state before and after spontaneous arousals from sleep in elderly and middle-aged women. Neuroscience 175:184–197.

Burke JF, Long NM, Zaghloul KA, Sharan AD, Sperling MR, Kahana MJ (2014) Human intracranial high-frequency activity maps episodic memory formation in space and time. NeuroImage 85:834–843.

Buzsáki G (2011) *Rhythms of the brain*. Oxford; New York: Oxford University Press.

Cantero JL, Atienza M, Madsen JR, Stickgold R (2004) Gamma EEG dynamics in neocortex and hippocampus during human wakefulness and sleep. NeuroImage 22:1271–1280.

Castelhano J, Duarte IC, Abuhaiba SI, Rito M, Sales F, Castelo-Branco M (2017) Cortical functional topography of high-frequency gamma activity relates to perceptual decision: an intracranial study. PLoS One 12: e0186428.

Cote KA, Lugt DR, Campbell KB (2002) Changes in the scalp topography of event-related potentials and behavioral responses during the sleep onset period. Psychophysiology 39:29–37.

De Gennaro L, Ferrara M, Curcio G, Cristiani R (2001) Antero-posterior EEG changes during the wakefulness–sleep transition. Clin Neurophysiol 112: 1901–1911.

Dickey CW, et al. (2022) Widespread ripples synchronize human cortical activity during sleep, waking, and memory recall. Proc Natl Acad Sci U S A 119:e2107797119.

Donoghue T, et al. (2020) Parameterizing neural power spectra into periodic and aperiodic components. Nat Neurosci 23:1655–1665.

Drouin S, et al. (2016) IBIS: an OR ready open-source platform for image-guided neurosurgery. Int J Comput Assist Radiol Surg 12:363–378.

Ferrara M, De Gennaro L (2011) Going local: insights from EEG and stereo-EEG studies of the human sleep-wake cycle. Curr Top Med Chem 11:2423–2437.
Flamand M, Boudet S, Lopes R, Vignal J-P, Reyns N, Charley-Monaca C, Peter-Derex L, Szurhaj W (2018) Confusional arousals during non-rapid eye movement sleep: evidence from intracerebral recordings. Sleep 41: zsy139.
Frauscher B, von Ellenrieder N, Dubeau F, Gotman J (2015a) Scalp spindles are associated with widespread intracranial activity with unexpectedly low synchrony. NeuroImage 105:1–12.
Frauscher B, von Ellenrieder N, Ferrari-Marinho T, Avoli M, Dubeau F, Gotman J (2015b) Facilitation of epileptic activity during sleep is mediated by high amplitude slow waves. Brain 138:1629–1641.
Frauscher B, et al. (2018a) Atlas of the normal intracranial electroencephalogram: neurophysiological awake activity in different cortical areas. Brain 141:1130–1144.
Frauscher B, von Ellenrieder N, Zelmann R, Rogers C, Nguyen DK, Kahane P, Dubeau F, Gotman J (2018b) High-frequency oscillations in the normal human brain. Ann Neurol 84:374–385.
Frauscher B, von Ellenrieder N, Dolezalova I, Bouhadoun S, Gotman J, Peter-Derex L (2020) Rapid eye movement sleep sawtooth waves are associated with widespread cortical activations. J Neurosci 40:8900–8912.
Greenberg JA, Burke JF, Haque R, Kahana MJ, Zaghloul KA (2015) Decreases in theta and increases in high frequency activity underlie associative memory encoding. NeuroImage 114:257–263.
Halász P (1998) Hierarchy of micro-arousals and the microstructure of sleep. Clin Neurophysiol 28:461–475.
Halász P, Kundra O, Rajna P, Pál I, Vargha M (1979) Micro-arousals during nocturnal sleep. Acta Physiol Acad Sci Hung 54:1–12.
Halasz P, Terzano M, Parrino L, Bodizs R (2004) The nature of arousal in sleep. J Sleep Res 13:1–23.
Huber R, Felice Ghilardi M, Massimini M, Tononi G (2004) Local sleep and learning. Nature 430:78–81.
Jain SV, Glauser TA (2013) Effects of epilepsy treatments on sleep architecture and daytime sleepiness: an evidence-based review of objective sleep metrics. Epilepsia 55:26–37.
Jasper H, Penfield W (1949) Electrocorticograms in man: effect of voluntary movement upon the electrical activity of the precentral gyrus. Arch Psychiatr Nervenkr 183:163–174.
Kaufman AB, Rosenthal R (2009) Can you believe my eyes? The importance of interobserver reliability statistics in observations of animal behaviour. Anim Behav 78:1487–1491.
Kemp B, van Someren P, Roessen M, van Dijk JG (2013) Assessment of human sleep depth is being de-standardized by recently advised EEG electrode locations Bazhenov M, ed. PLoS One 8:e71234.
Krueger JM, Rector DM, Roy S, Van Dongen HPA, Belenky G, Panksepp J (2008) Sleep as a fundamental property of neuronal assemblies. Nat Rev Neurosci 9:910–919.
Kucewicz MT, et al. (2014) High frequency oscillations are associated with cognitive processing in human recognition memory. Brain 137:2231–2244.
Landman BA, Warfield SK (2012) MICCAI 2012: workshop on multi-atlas labeling.
Latreille V, von Ellenrieder N, Peter-Derex L, Dubeau F, Gotman J, Frauscher B (2020) The human K-complex: insights from combined scalp-intracranial EEG recordings. NeuroImage 213:116748.
Latreille V, Avigdor T, Thomas J, Crane J, Sziklas V, Jones-Gotman M, Frauscher B (2023) Scalp and hippocampal sleep correlates of memory function in drug-resistant temporal lobe epilepsy. Sleep 47:zsad228.
Lendner JD, Helfrich RF, Mander BA, Romundstad L, Lin JJ, Walker MP, Larsson PG, Knight RT (2020) An electrophysiological marker of arousal level in humans. eLife 9:e55092.
Liu AA, et al. (2022) A consensus statement on detection of hippocampal sharp wave ripples and differentiation from other fast oscillations. Nat Commun 13:6000.
Lundqvist M, Rose J, Herman P, Brincat SL, Buschman TJ, Miller EK (2016) Gamma and beta bursts underlie working memory. Neuron 90:152–164.
Mahowald MW, Schenck CH (2005) Insights from studying human sleep disorders. Nature 437:1279–1285.
Mainieri G, Loddo G, Castelnovo A, Balella G, Cilea R, Mondini S, Manconi M, Provini F (2022) EEG activation does not differ in simple and complex episodes of disorders of arousal: a spectral analysis study. Nat Sci Sleep 14: 1097–1111.
Mathur R, Douglas NJ (1995) Frequency of EEG arousals from nocturnal sleep in normal subjects. Sleep 18:330–333.
Meyer S, et al. (2016) Voxel-based lesion-symptom mapping of stroke lesions underlying somatosensory deficits. NeuroImage Clin 10:257–266.
Mikulan E, Hesse E, Sedeño L, Bekinschtein T, Sigman M, del Carmen García M, Silva W, Ciraolo C, García AM, Ibáñez A (2018) Intracranial high-γ connectivity distinguishes wakefulness from sleep. NeuroImage 169: 265–277.
Mitterling T, Högl B, Schönwald SV, Hackner H, Gabelia D, Biermayr M, Frauscher B (2015) Sleep and respiration in 100 healthy Caucasian sleepers—a polysomnographic study according to American academy of sleep medicine standards. Sleep 38:867–875.
Neckelmann D, Ursin R (1993) Sleep stages and EEG power spectrum in relation to acoustical stimulus arousal threshold in the rat. Sleep 16:467–477.
Nelson MJ, et al. (2017) Neurophysiological dynamics of phrase- structure building during sentence processing. Proc Natl Acad Sci U S A 114: E3669–E3678.
Nobili L, Ferrara M, Moroni F, De Gennaro L, Russo GL, Campus C, Cardinale F, De Carli F (2011) Dissociated wake-like and sleep-like electro-cortical activity during sleep. NeuroImage 58:612–619.
Nourski KV, Steinschneider M, Rhone AE, Howard MA 3rd (2017) Intracranial electrophysiology of auditory selective attention associated with speech classification tasks. Front Hum Neurosci 10:691.
Oane I, et al. (2020) Cingulate cortex function and multi-modal connectivity mapped using intracranial stimulation. NeuroImage 220:117059.
Omigie D, Pearce M, Lehongre K, Hasboun D, Navarro V, Adam C, Samson S (2019) Intracranial recordings and computational modeling of music reveal the time course of prediction error signaling in frontal and temporal cortices. J Cogn Neurosci 31:855–873.
Parrino L, Halasz P, Tassinari CA, Terzano MG (2006) CAP, epilepsy and motor events during sleep: the unifying role of arousal. Sleep Med Rev 10:267–285.
Peter-Derex L, Magnin M, Bastuji H (2015) Heterogeneity of arousals in human sleep: a stereo-electroencephalographic study. NeuroImage 123: 229–244.
Peter-Derex L, Klimes P, Latreille V, Bouhadoun S, Dubeau F, Frauscher B (2020) Sleep disruption in epilepsy: ictal and interictal epileptic activity matter. Ann Neurol 88:907–920.
Peter-Derex L, Avigdor T, Rheims S, Guénot M, von Ellenrieder N, Gotman J, Frauscher B (2023a) Enhanced thalamocortical functional connectivity during REM sleep sawtooth waves. Sleep 46:zsad097.
Peter-Derex L, von Ellenrieder N, van Rosmalen F, Hall J, Dubeau F, Gotman J, Frauscher B (2023b) Regional variability in intracerebral properties of NREM to REM sleep transitions in humans. Proc Natl Acad Sci U S A 120:e2300387120.
Ruby P, Eskinazi M, Bouet R, Rheims S, Peter-Derex L (2021) Dynamics of hippocampus and orbitofrontal cortex activity during arousing reactions from sleep: an intracranial electroencephalographic study. Hum Brain Mapp 42:5188–5203.
Schieber J, Muzet A, Ferierre P (1971) Les phases d'activation transitoire spontanees au cours du sommeil chez l'homme. Arch Sci Physiol 25: 443–465.
Setzer B, Fultz NE, Gomez DEP, Williams SD, Bonmassar G, Polimeni JR, Lewis LD (2022) A temporal sequence of thalamic activity unfolds at transitions in behavioral arousal state. Nat Commun 13:5442.
Sforza E, Nicolas A, Lavigne G, Gosselin A, Petit D, Montplaisir J (1999) EEG and cardiac activation during periodic leg movements in sleep. Neurology 52:786–786.
Sforza E, Jouny C, Ibanez V (2000) Cardiac activation during arousal in humans: further evidence for hierarchy in the arousal response. Clin Neurophysiol 111:1611–1619.
Shvarts V, Chung S (2013) Epilepsy, antiseizure therapy, and sleep cycle parameters. Epilepsy Res Treat 2013:1–8.
Stephan AM, Lecci S, Cataldi J, Siclari F (2021) Conscious experiences and high-density EEG patterns predicting subjective sleep depth. Curr Biol 31:5487–5500.
Tadel F, Baillet S, Mosher JC, Pantazis D, Leahy RM (2011) Brainstorm: a user-friendly application for MEG/EEG analysis. Comput Intell Neurosci 2011:1–13.
Terzaghi M, Sartori I, Tassi L, Didato G, Rustioni V, LoRusso G, Manni R, Nobili L (2009) Evidence of dissociated arousal states during NREM parasomnia from an intracerebral neurophysiological study. Sleep 32: 409–412.

Terzano MG, Parrino L, Boselli M, Smerieri A, Spaggiari MC (2000) CAP components and EEG synchronization in the first 3 sleep cycles. Clin Neurophysiol 111:283–290.

Terzano MG, Parrino L, Rosa A, Palomba V, Smerieri A (2002) CAP and arousals in the structural development of sleep: an integrative perspective. Sleep Med 3:221–229.

Terzano MG, Parrino L, Smerieri A, Carli F, Nobili L, Donadio S, Ferrillo F (2005) CAP and arousals are involved in the homeostatic and ultradian sleep processes. J Sleep Res 14:359–368.

Thampratankul L, Nagasawa T, Rothermel R, Juhasz C, Sood S, Asano E (2010) Cortical gamma oscillations modulated by word association tasks: intracranial recording. Epilepsy Behav 18:116–118.

von Ellenrieder N, Gotman J, Zelmann R, Rogers C, Nguyen DK, Kahane P, Dubeau F, Frauscher B (2020) How the human brain sleeps: direct cortical recordings of normal brain activity. Ann Neurol 87: 289–301.

Younes M, Schweitzer PK, Griffin KS, Balshaw R, Walsh JK (2020) Comparing two measures of sleep depth/intensity. Sleep 43:zsaa127.